

11-19-2021


Metabolic adaptation to the chronic loss of Ca²⁺ signaling induced by KO of IP₃ receptors or the mitochondrial Ca²⁺ uniporter

Michael P. Young
Thomas Jefferson University

Zachary T Schug
The Wistar Institute

David M. Booth
Thomas Jefferson University

David I Yule
Follow this and additional works at: <https://jdc.jefferson.edu/pacbfp>
University of Rochester

 Part of the [Medical Anatomy Commons](#), [Medical Cell Biology Commons](#), and the [Pathology Commons](#)
Katsuhiko Mikoshiba
Shanghai Tech University

Recommended Citation

See next page for additional authors

Young, Michael P.; Schug, Zachary T; Booth, David M.; Yule, David I; Mikoshiba, Katsuhiko; Hajnóczky, György; and Joseph, Suresh K, "Metabolic adaptation to the chronic loss of Ca²⁺ signaling induced by KO of IP₃ receptors or the mitochondrial Ca²⁺ uniporter" (2021).
Department of Pathology, Anatomy, and Cell Biology Faculty Papers. Paper 339.
<https://jdc.jefferson.edu/pacbfp/339>

This Article is brought to you for free and open access by the Jefferson Digital Commons. The Jefferson Digital Commons is a service of Thomas Jefferson University's [Center for Teaching and Learning \(CTL\)](#). The Commons is a showcase for Jefferson books and journals, peer-reviewed scholarly publications, unique historical collections from the University archives, and teaching tools. The Jefferson Digital Commons allows researchers and interested readers anywhere in the world to learn about and keep up to date with Jefferson scholarship. This article has been accepted for inclusion in Department of Pathology, Anatomy, and Cell Biology Faculty Papers by an authorized administrator of the Jefferson Digital Commons. For more information, please contact: JeffersonDigitalCommons@jefferson.edu.

Authors




Michael P. Young, Zachary T Schug, David M. Booth, David I Yule, Katsuhiko Mikoshiba, György Hajnóczky, and Suresh K Joseph



Metabolic adaptation to the chronic loss of Ca²⁺ signaling induced by KO of IP₃ receptors or the mitochondrial Ca²⁺ uniporter

Received for publication, April 18, 2021, and in revised form, October 4, 2021. Published, Papers in Press, November 19, 2021,

<https://doi.org/10.1016/j.jbc.2021.101436>

Michael P. Young¹, Zachary T. Schug² , David M. Booth¹, David I. Yule³ , Katsuhiko Mikoshiba^{4,5}, György Hajnóczky¹ , and Suresh K. Joseph^{1,*}

From the ¹Department of Pathology, MitoCare Center, Anatomy, and Cell Biology, Thomas Jefferson University, Philadelphia, Pennsylvania, USA; ²Molecular and Cellular Oncogenesis, The Wistar Institute, Philadelphia, Pennsylvania, USA; ³Department of Pharmacology & Physiology, University of Rochester, Rochester, New York, USA; ⁴Shanghai Institute of Advanced Immunochemical Studies (SIAIS), Shanghai Tech University, Shanghai, China; ⁵Department of Biomolecular Science, Faculty of Science, Toho University, Funabashi, Japan

Edited by Roger Colbran

Calcium signaling is essential for regulating many biological processes. Endoplasmic reticulum inositol trisphosphate receptors (IP₃R) and the mitochondrial Ca²⁺ uniporter (MCU) are key proteins that regulate intracellular Ca²⁺ concentration. Mitochondrial Ca²⁺ accumulation activates Ca²⁺-sensitive dehydrogenases of the tricarboxylic acid (TCA) cycle that maintain the biosynthetic and bioenergetic needs of both normal and cancer cells. However, the interplay between calcium signaling and metabolism is not well understood. In this study, we used human cancer cell lines (HEK293 and HeLa) with stable KOs of all three IP₃R isoforms (triple KO [TKO]) or MCU to examine metabolic and bioenergetic responses to the chronic loss of cytosolic and/or mitochondrial Ca²⁺ signaling. Our results show that TKO cells (exhibiting total loss of Ca²⁺ signaling) are viable, displaying a lower proliferation and oxygen consumption rate, with no significant changes in ATP levels, even when made to rely solely on the TCA cycle for energy production. MCU KO cells also maintained normal ATP levels but showed increased proliferation, oxygen consumption, and metabolism of both glucose and glutamine. However, MCU KO cells were unable to maintain ATP levels and died when relying solely on the TCA cycle for energy. We conclude that constitutive Ca²⁺ signaling is dispensable for the bioenergetic needs of both IP₃R TKO and MCU KO human cancer cells, likely because of adequate basal glycolytic and TCA cycle flux. However, in MCU KO cells, the higher energy expenditure associated with increased proliferation and oxygen consumption makes these cells more prone to bioenergetic failure under conditions of metabolic stress.

Ca²⁺ signaling plays an important role in regulating many diverse biological processes ranging from cell proliferation, secretion, motility, metabolism, and cell death (1). A key event that initiates Ca²⁺ signaling is the release of Ca²⁺ from intracellular stores by the three isoforms of inositol

trisphosphate receptor (IP₃R) channels (2). The depletion of internal Ca²⁺ stores secondarily stimulates Ca²⁺ entry *via* Orai channels in the plasma membrane. Thus, loss of IP₃R-mediated Ca²⁺ signaling would block both the intracellular and extracellular components of agonist-mediated Ca²⁺ signaling. An increase of cytosolic Ca²⁺ in the environment of the mitochondria facilitates Ca²⁺ uptake into the matrix by a complex of inner membrane proteins of which the mitochondrial Ca²⁺ uniporter (MCU) is the pore-forming constituent (3). The elevations of Ca²⁺ in the cytosol and mitochondrial compartments act on multiple effector proteins to alter cell function (1, 4). In the mitochondrial matrix, Ca²⁺ stimulates the activity of three dehydrogenases of the tricarboxylic acid (TCA) cycle (5), respiratory complexes (6), and ATP synthase (7) to enhance ATP generation. Higher matrix Ca²⁺ accumulation can open the permeability transition pore and cause cell death (8). Inactivating the function of all three IP₃R isoforms or MCU channels would therefore be expected to have wide-ranging effects, including compromising the metabolic and bioenergetic status of the cells.

Global and conditional KO mouse models of individual IP₃R isoforms have provided valuable information on the role of Ca²⁺ signaling in regulating organ function (9–14). However, functional redundancy and postnatal mortality have complicated these studies (15–19). Few studies have examined the effects of the conditional deletion of all three IP₃R isoforms. In hematopoietic cells, these investigations indicated a critical role for Ca²⁺ in regulating early developmental checkpoints in T and B lymphocytes (20, 21). In mouse embryonic stem cells, the IP₃R TKO cells showed enhanced differentiation into the cardiomyocyte lineage and impaired differentiation into the hematopoietic lineage (22). Inducible KOs of all IP₃R isoforms in mouse vascular endothelial cells (14) or smooth muscle cells (13) have been shown to affect basal blood pressure and vascular tone.

Studying the mechanisms of adaptation to a loss of Ca²⁺ signaling is much easier in cultured cell systems than in animal

* For correspondence: Suresh K. Joseph, suresh.joseph@jefferson.edu.

Metabolic adaptation to loss of calcium signaling

KO models. A widely used cell culture model is a chicken DT40 cell line in which all three IP₃R isoforms have been disrupted (23). However, studies using DT40 cells have primarily focused on the structure, function, and regulation of IP₃Rs (24). A number of reports have noted that DT40 IP₃R TKO cells have a baseline increase in autophagy (25–27). Cardenas *et al.* (27) proposed that the increased autophagy compensated for the bioenergetic deficit caused by the loss of endoplasmic reticulum (ER)/mitochondrial Ca²⁺ signaling required to maintain optimal operation of the TCA cycle. Cardenas *et al.* (28, 29) have extended these studies to compare the effects of acute inhibition of ER/mitochondrial Ca²⁺ transfer in normal and cancer cells. They concluded that, unlike normal cells, the stimulation of autophagy in cancer cells is not sufficient to compensate for the increased energy demand of uncontrolled growth, with cell death resulting from a “bioenergetic crisis” during mitosis. The advent of new methods of gene disruption has enabled all three IP₃R isoforms to be deleted in human embryonic kidney 293 (HEK293) (30, 31) and HeLa (32) human cancer cell lines. While these KO cells have primarily been used as an expression system to study the functional properties of IP₃R mutants, they also offer the opportunity to investigate the metabolic and bioenergetic consequences of the chronic effects of a total loss of Ca²⁺ signaling. This is the primary objective of the present investigation.

Many studies have examined the physiological consequences of disrupting mitochondrial Ca²⁺ signaling using global and tissue-specific MCU KO mouse models. In most cases, a relatively mild phenotype at baseline has been observed in tissues, such as the heart (33), skeletal muscle (34), exocrine pancreas (35), endocrine pancreas (36), brown adipose tissue (37), and photoreceptors (38) suggesting the existence of robust adaptive mechanisms that have yet to be fully characterized, including upregulation of alternative mechanisms of mitochondrial Ca²⁺ transport. Where metabolic changes have been investigated in MCU KOs, the results have generally been tissue specific. For example, fatty acid oxidation is increased in cardiac (39) and skeletal muscle (34), and decreased in liver (40) and pulmonary macrophages (41). Relatively few studies have examined the metabolic or bioenergetic consequences of knocking out MCU in cultured cells. Using RNA interference, it was concluded that MCU was dispensable for growth in a breast cancer cell line (42) but stimulated the growth and metastasis of hepatocellular carcinoma (43) and colorectal cancer cells (44). Silencing of MCU in mouse pancreatic β-cells suppressed the increase of ATP/ADP induced by glucose (45). The absence of MCU in vascular smooth muscle cells impaired mitochondrial fusion and entry into the G1/S phase of the cell cycle (46). The conditional deletion of MCU from mouse embryonic fibroblasts (MEFs) enhanced differentiation to myofibroblasts by an epigenetic mechanism that involves enhanced glycolysis and increased accumulation of α-ketoglutarate (α-KG) (47). Overall, it is clear that the metabolic phenotype of the MCU KO cells is dependent on the cell type being investigated. To obtain a clearer picture of the metabolic consequences of disrupting

either ER or mitochondrial Ca²⁺, we have carried out the present study in which IP₃Rs or MCU have been knocked out in the same human cancer cell lines. Our studies show that the IP₃R TKO cells have adapted to the total loss of Ca²⁺ signaling with a lower proliferation and oxygen consumption rate (OCR), but no significant changes in adenine nucleotides, even when artificially made to rely entirely on the TCA cycle for their bioenergetic and biosynthetic needs. By contrast, the loss of MCU is associated with an increased proliferation and OCR, increased metabolism of glucose and glutamine, a higher level of basal AMP-dependent kinase (AMPK), and bioenergetic failure when made to rely solely on the TCA cycle. We conclude that baseline rates of aerobic glycolysis and the TCA cycle are sufficient to make constitutive ER/mitochondrial Ca²⁺ signaling dispensable for the growth and function of both IP₃R TKO and MCU KO cancer cells. However, in MCU KO cells, the higher energy expenditure associated with increased proliferation and oxygen consumption make these cells more prone to bioenergetic failure under conditions of metabolic stress.

Results

Cytosolic and mitochondrial Ca²⁺

We initially characterized cytosolic Ca²⁺ signals in the IP₃R and MCU KO HEK293 cell models incubated in the absence of extracellular Ca²⁺. As expected, the loss of all three IP₃R isoforms prevented any cytosolic Ca²⁺ changes induced by carbachol (Cch) stimulation of endogenous muscarinic receptors (Fig. 1, A and B). MCU deletion was carried out in the variant HEK293T cell line (48), and these cells showed a decreased Cch-mediated cytosolic Ca²⁺ signal when compared with the appropriate control of WT HEK293T cells. The cytosolic Ca²⁺ responses of WT HEK293 and HEK293T cells were not significantly different (Fig. 1A), and this also proved to be the case for several other parameters measured in this study. This includes cell growth (Fig. 2A), glucose utilization (Fig. S1A), glutamine consumption (Fig. S1B), total NAD⁺ and NADH (Fig. S1, C and D), lactate accumulation (Fig. S1E), ATP levels (Fig. S1F), phosphorylated AMPK levels (Fig. S1G), and phosphorylated pyruvate dehydrogenase (p-PDH) levels (Fig. S1H). Hence, only the WT HEK293 cells are represented as controls in most of the remaining figures.

The ability of mitochondria to sequester and release a 50 μM pulse of Ca²⁺ in saponin-permeabilized cell lines was measured in Figure 1, C and D. Both WT and IP₃R TKO cells had comparable rates of mitochondrial uptake and (carbonylcyanide-4-(trifluoromethoxy)phenylhydrazone) (FCCP)-induced release compared with the negligible rates for both processes seen in the MCU KO cells. The MCU KO-permeabilized cells consistently showed an elevated steady state [Ca²⁺] in the medium prior to Ca²⁺ pulse addition. This may reflect the failure of the cells to sequester the endogenous contaminating Ca²⁺ into the mitochondria before the initiation of the experiment. The mitochondrial Ca²⁺ content in intact cells was estimated using the ratiometric, high-

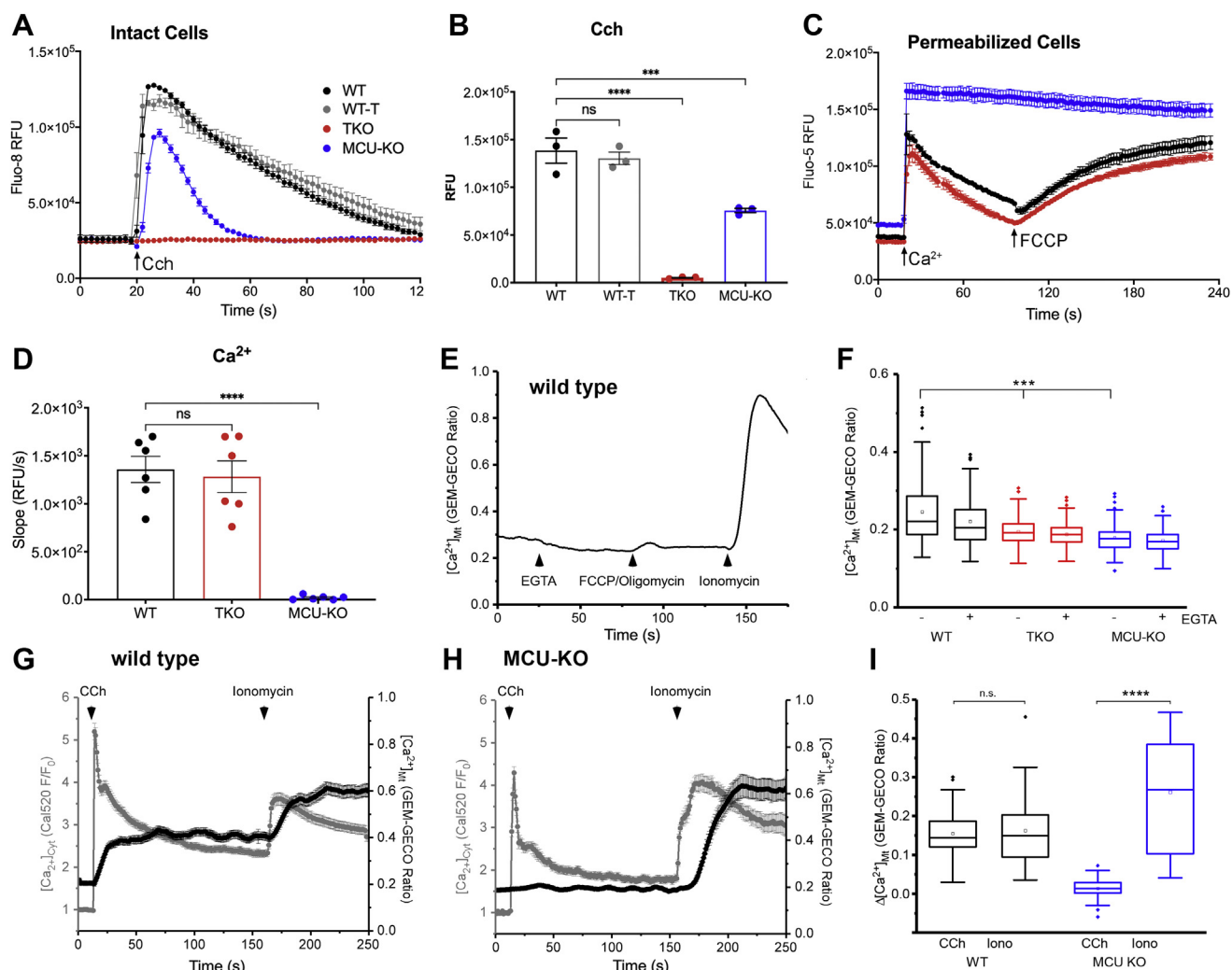


Figure 1. Measurements of cytosolic and mitochondrial Ca²⁺ content in WT, IP₃R TKO, and MCU-KO HEK293T cells. *A*, cytosolic Ca²⁺ changes in response to 25 μM Cch was measured in the absence of external Ca²⁺. The data shown are from a representative experiment and are the mean ± SEM of four replicates for each cell type. *B*, the quantitation of the amplitude of the changes in cytosolic Ca²⁺. The data are the mean ± SEM of three independent experiments, each carried out in triplicate; **p* < 0.05; ***p* < 0.01; ****p* < 0.001; *****p* < 0.0001, one-way ANOVA followed by multiple comparison analysis using Dunnett's test. *C*, cells were permeabilized with saponin, and the clearance of a 50 μM pulse of Ca²⁺ added at 18 s was measured as described in the "Experimental procedures" section. A further addition of 1 μM FCCP was made at 100 s. *C*, from a representative experiment. *D*, a quantitation in which the initial rate of Ca²⁺ uptake over a 20 s period was calculated as given in (*B*) (*n* = 6). *E*, representative trace of epifluorescence single-cell recordings of GEM-GECO emission ratio in WT HEK293 showing matrix Ca²⁺ ([Ca²⁺]_{Mt}) in response to the removal/chelation of [Ca²⁺]_{Ext} with EGTA (10 mM) and in response to FCCP (5 μM) and oligomycin (1 μg/ml) was measured. The subsequent addition of ionomycin (10 μM) was used as a uniporter-independent positive control for [Ca²⁺]_{Mt}. *F*, the quantification of [Ca²⁺]_{Mt} in the presence and absence of EGTA as measured by GEM-GECO emission ratio in WT, TKO, and MCU-KO cells. Box plots show mean, median, interquartile range, and outlier markers. ****p* < 0.001, one-way ANOVA followed by multiple comparison analysis using Dunnett's test. *G* and *H*, simultaneous [Ca²⁺]_{Cyt} (Cal520) (gray traces) and [Ca²⁺]_{Mt} (GEM-GECO emission ratio) in response to addition of carbachol (CCh) and ionomycin to WT (*G*) and MCU-KO (*H*) HEK cells. The sustained elevation of mitochondrial Ca²⁺ signal in (*G*) is probably because of the asynchronous oscillations of [Ca²⁺]_{Cyt} observed in single cells after the initial rise of Ca²⁺ (not shown). *I*, box plot quantification of Δ[Ca²⁺]_{Mt} from individual cell recordings in (*G*) and (*H*). Responses are plotted as [Ca²⁺]_{Mt} peak (0–150 s) – [Ca²⁺]_{Mt} baseline for CCh stimulation and [Ca²⁺]_{Mt} peak *t* > 150 s – [Ca²⁺]_{Mt} plateau at *t* = 150 s for ionomycin. *****p* < 0.0001 Wilcoxon signed-rank test. FCCP, (carbonylcyanide-4-(trifluoromethoxy)phenyl)hydrazine; HEK293T, human embryonic kidney 293T cell line; IP₃R, inositol trisphosphate receptor; MCU, mitochondrial Ca²⁺ uniporter; TKO, triple KO.

affinity, genetically encoded, fluorescent probe GEM-GECO (*K_d* ~340 nM; (49)). The baseline signal in all three cell lines was not significantly decreased by chelation of extracellular Ca²⁺ or by depolarization with FCCP/oligomycin, indicating that there is very little Ca²⁺ in the mitochondria under unstimulated conditions (Fig. 1, *E* and *F*). The measured basal content was only marginally lower (~20%) in IP₃R TKO and MCU KO cells (Fig. 1*F*). It should be noted that a variable lowering of mitochondrial Ca²⁺ content has been reported in mouse MCU KO models (50–53). The

ability of the probe to register increases in mitochondrial Ca²⁺ was verified by measuring responses to ionomycin and Cch (Fig. 1, *E*, *G*, and *H*). Parallel measurements of cytoplasmic and mitochondrial Ca²⁺ confirmed that Cch-induced increases in mitochondrial Ca²⁺ were suppressed in the MCU KO cells (Fig. 1, *G*–*I*). Taken together, the results show that IP₃R TKO cells have lost agonist-mediated cytosolic Ca²⁺ signaling but retain the ability to sequester mitochondrial Ca²⁺, whereas the MCU KO cells have retained cytosolic Ca²⁺ signaling (albeit at a reduced level) but have lost

Metabolic adaptation to loss of calcium signaling

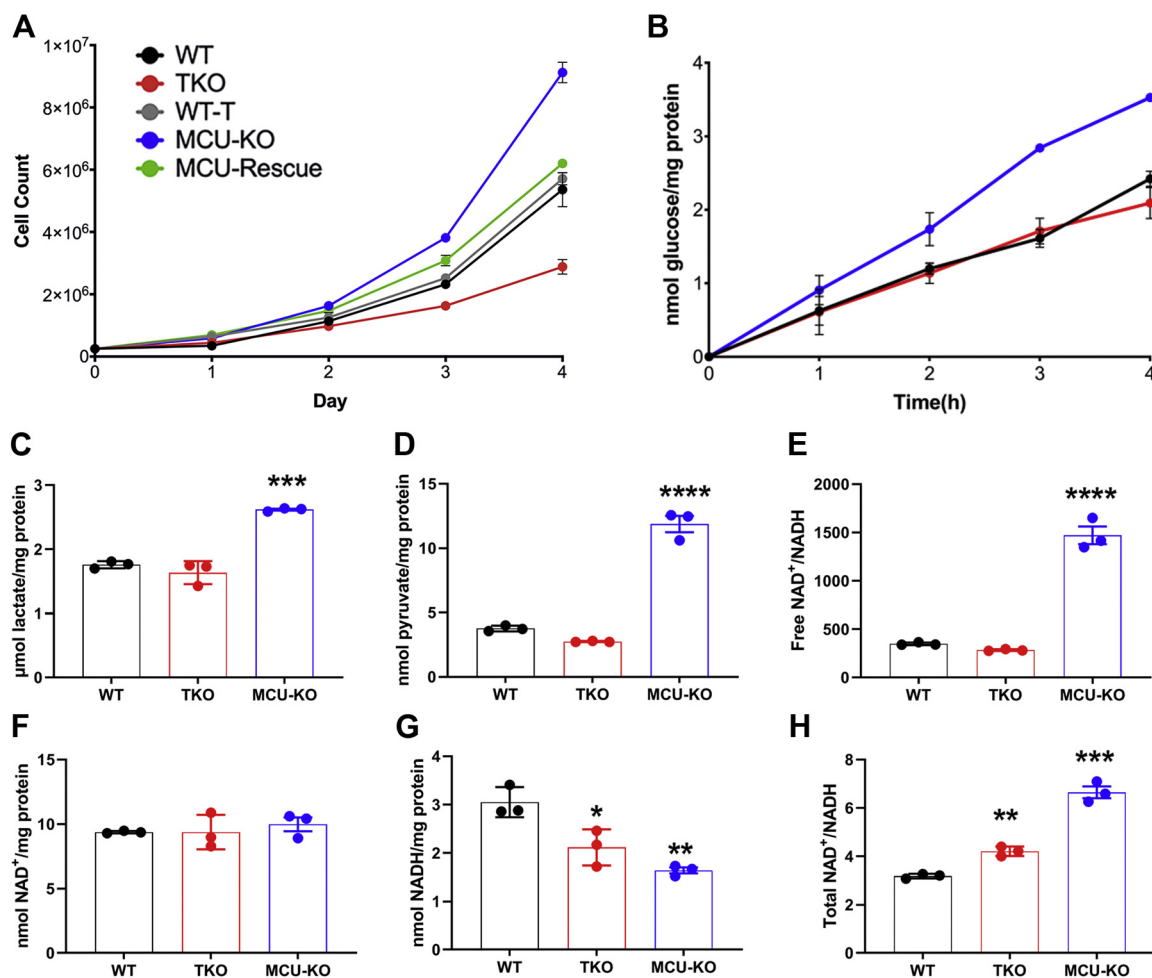


Figure 2. Growth, glycolysis, and pyridine nucleotide levels in WT, IP₃R TKO, and MCU-KO HEK293T cells. A, growth curves of the indicated HEK293 cell lines were measured. The data shown are the mean ± SEM of three experiments. B, the media from cells grown for 4 to 5 days were replaced with DMEM containing 5 mM glucose instead of 25 mM glucose. Aliquots of the media sampled at the times indicated were assayed for glucose. The data shown are the mean ± SEM of four experiments. C, cells were deproteinized in 0.6 M perchloric acid, and neutralized lysates were assayed for lactate. D, as in (C), but pyruvate was measured. The cytosolic-free NAD⁺/NADH ratio was calculated from the lactate/pyruvate ratio (E). Total NAD⁺ (F) and NADH (G) were measured by an enzymatic cycling procedure. The total NAD⁺/NADH ratio is quantitated in (H). For (C–H), the data are the mean ± SEM of three independent experiments, each carried out in triplicate; **p* < 0.05; ***p* < 0.01; ****p* < 0.001; *****p* < 0.0001, one-way ANOVA followed by multiple comparison analysis using Dunnett's test. DMEM, Dulbecco's modified Eagle's medium; HEK293T, human embryonic kidney 293T cell line; IP₃R, inositol trisphosphate receptor; MCU, mitochondrial Ca²⁺ uniporter; TKO, triple KO.

mitochondrial Ca²⁺ uptake. The impact of these Ca²⁺ signaling phenotypes on metabolism and bioenergetics is investigated later.

Cell growth and glucose metabolism

A number of basic growth and metabolic parameters were measured in the HEK293 cell lines (Fig. 2). In the Dulbecco's modified Eagle's medium (DMEM) growth medium (containing glucose [25 mM], glutamine [5 mM], and pyruvate [1 mM]), the IP₃R TKO cells grew more slowly, and the MCU KO cells grew more rapidly, than their corresponding WT counterpart (Fig. 2A). The cells were entirely dependent on glucose and glutamine as fuels, since the omission of either substrate prevented growth in all the cell lines (not shown). Glucose consumption was measured at a lower glucose concentration of 5 mM and found to be comparable between WT and IP₃R TKO cells (Fig. 2B). However, the MCU KO cells

consumed glucose more rapidly (Fig. 2B). Both cellular lactate (Fig. 2C) and pyruvate (Fig. 2D) showed increased levels in the MCU KO cells. The assumption of near equilibrium of the lactate dehydrogenase (LDH) reaction allows calculation of the free cytosolic NAD⁺/NADH ratio from the pyruvate/lactate ratio (54). This calculation indicated a substantial increase in the NAD⁺/NADH ratio in MCU KO cells (Fig. 2E). To verify these findings, the total cellular levels of NAD⁺ and NADH were also measured directly by an enzymatic cycling method (Fig. 2, F and G). Significant changes in NAD⁺ levels were not observed, but the levels of NADH decreased substantially in MCU KO cells and to a lesser extent in IP₃R TKO cells (Fig. 2G). Similar changes were also observed for NADP⁺/NADPH (Fig. S2A). Quantitation of the total levels of metabolites by mass spectroscopy showed that MCU KO cells have increased levels of glutamate, α-KG, and citrate (Fig. S2B). These metabolite changes are consistent with increased metabolism of glutamine in MCU KO cells. Similar

increases in α -KG have been noted in MCU KO fibroblasts (47) and photoreceptors (38). In fibroblasts, the increase in α -KG was attributed to enhanced glutamine metabolism and linked to epigenetic changes altering the methylation of histones. In photoreceptors, enhanced glutamine metabolism was not observed. Both malate and aspartate levels were decreased in the MCU KO HEK cells (Fig. S2B). The fall in aspartate could in part be related to increased utilization, since large increases were observed in carbamoyl aspartate (used in pyrimidine synthesis) and asparagine levels. The fall in malate is expected, since malate is in equilibrium with aspartate through oxaloacetate. The fall in these metabolites may disrupt the malate/aspartate shuttle and may account for the increased reliance on lactate production as a means of regenerating the

NAD⁺ required for glycolysis. Overall, these results indicate that there are marked increases in growth rate, glycolysis, and NAD⁺/NADH redox state in the MCU KO cells.

Key bioenergetic parameters in WT, IP₃R TKO, and MCU KO cells

Altered supply of NADH by dehydrogenases and/or utilization by the respiratory chain may underlie the observed changes in NAD⁺/NADH ratio. This prompted us to examine the OCR of the KO cell lines (Fig. 3, A and B). In intact cells exposed to complete growth medium, the basal OCR of MCU KO cells was increased by ~60% relative to WT cells. Under the same conditions, the OCR of IP₃R TKO cells was

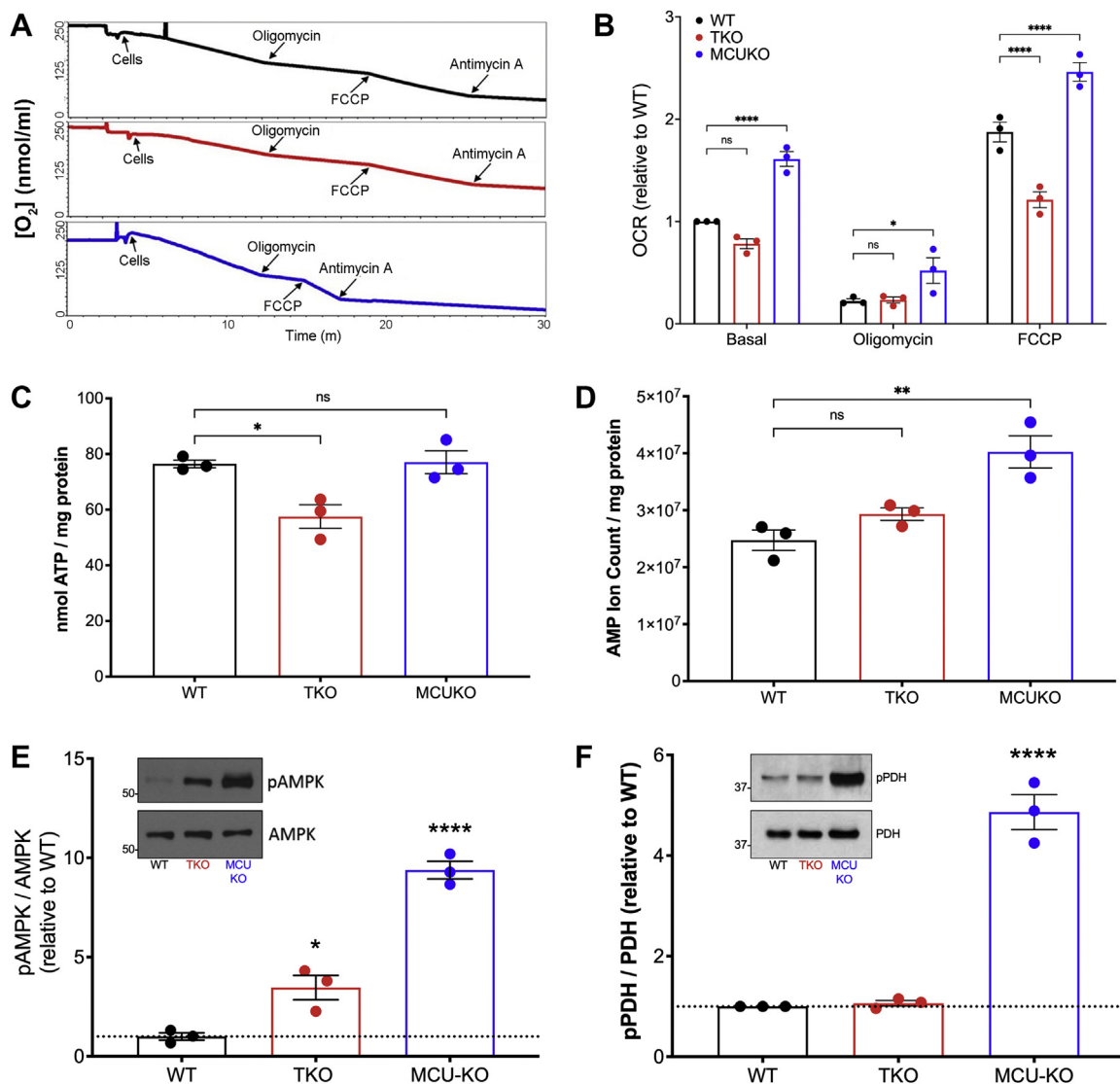


Figure 3. Some bioenergetic parameters of HEK293 KO cells. *A*, equal amounts of cells (10^6) incubated in complete DMEM were added to the chamber of an O₂ electrode, and rates of O₂ consumption (OCR) were measured under basal conditions and after the sequential additions of oligomycin (1 μ g/ml), FCCP (1 μ M), and antimycin A (2 μ M). *B*, quantification of OCR is shown normalized to the basal OCR of WT cells. The data are the mean + SEM of three independent experiments, each carried out in triplicate: * $p < 0.05$; ** $p < 0.01$; *** $p < 0.001$; **** $p < 0.0001$, two-way ANOVA followed by multiple comparison analysis using Dunnett's test. *C*, ATP was measured in neutralized perchloric acid (PCA) lysates with a luciferase assay. *D*, AMP was measured in lysates processed for LC-MS/MS experiments. *E* and *F*, the phosphorylation status of AMPK and PDH measured by immunoblotting with phospho-specific antibodies. Values are normalized to the total levels of the enzymes. Statistical evaluation for (*C*–*F*) used one-way ANOVA with symbols as in (*B*). AMPK, AMP-dependent kinase; DMEM, Dulbecco's modified Eagle's medium; FCCP, (carbonyl)cyanide-4-(trifluoromethoxy)phenylhydrazone; HEK293, human embryonic kidney 293T cell line; OCR, oxygen consumption rate; PDH, pyruvate dehydrogenase.

Metabolic adaptation to loss of calcium signaling

decreased by ~25%. The same trends were observed when respiration was uncoupled with FCCP. Differences in OCR in intact cells could reflect altered availability of substrates to the respiratory chain. However, the decreased OCR in IP₃R TKO cells and increased OCR in MCU KO cells was also observed in permeabilized cells supplied with an excess of glutamate/malate and ADP (Fig. S2C). In the case of MCU KO cells, differences of OCR seen in intact cells in the presence of oligomycin or FCCP were not observed in permeabilized cells, suggesting that the differences seen in intact cells under these conditions may reflect enhanced substrate availability. We examined the ability of the cell lines to maintain basal ATP levels and found no statistical differences between the three cell lines (Fig. 3C). However, the basal AMP levels were substantially elevated in the MCU KO cells and to a smaller extent in IP₃R TKO cells (Fig. 3D). The different AMP levels correlated with the phosphorylation state of AMPK in the three cell lines (Fig. 3E). PDH is a key mitochondrial phosphoenzyme controlling the flow of glucose carbon into the TCA cycle and would therefore be one of many steps controlling NADH supply. The dephosphorylation and activation of PDH is catalyzed by a Ca²⁺-sensitive phosphatase (5). In agreement with other MCU KO models (34, 50, 55, 56), the phosphorylation of PDH is substantially increased in MCU KO HEK293T

cells. However, PDH phosphorylation was unaltered in IP₃R TKO cells (Fig. 3F).

Autophagy is a key cellular process regulated by the energy sensor AMPK (57). We therefore measured autophagy in the three cell lines by quantitating microtubule-associated protein 1 light chain 3 (LC3) conversion and p62 degradation detected by immunoblotting (Fig. 4). The data show increased levels of LC3-II (Fig. 4, A and B) and p62 (Fig. 4, C and D) in the IP₃R TKO cells but not in MCU KO cells. In order to distinguish between effects on enhanced autophagosome formation or decreased fusion with lysosomes, we blocked the latter process by preincubation of the cells with bafilomycin (58). The increase in LC3-II/p62 observed in IP₃R TKO cells was retained in the bafilomycin-treated cells with no additional changes seen in the MCU KO cells. The results are in line with several studies showing enhanced autophagy in IP₃R TKO DT40 lymphocytes that is AMPK independent ((25, 26); but see Ref. (27)). The data also show that the AMPK activation seen in MCU KO cells does not lead to enhanced autophagy.

Isotope tracer analysis

To investigate the metabolism of glucose in more detail, we used U-¹³C-glucose and mass spectroscopy. For the isotope

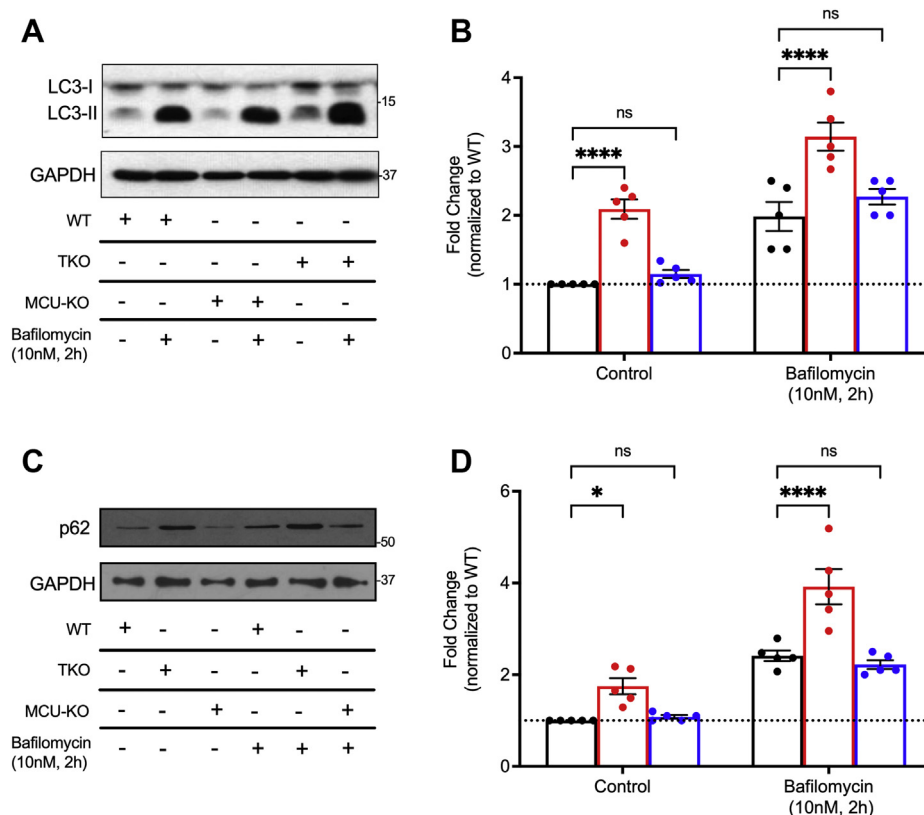


Figure 4. Autophagy is enhanced in IP₃R KO cells but not in MCU KO cells. A, cells grown for 4 to 5 days in nutrient-replete medium were analyzed by immunoblotting for LC3 in the presence or the absence of bafilomycin treatment (10 nM; 2 h). Quantitation of the LC3-II band is shown in B with data expressed relative to WT, untreated cells. C, lysates were immunoblotted for p62, and the data are quantitated in (D) with data expressed relative to WT, untreated cells. For (B) and (D), each point is an independent experiment performed in duplicate, error bars represent SEM, n = 5; **p* < 0.05; ***p* < 0.01; ****p* < 0.001; *****p* < 0.0001, two-way ANOVA followed by multiple comparison analysis using Dunnett's test. The data indicated no statistically significant interaction between the effects of cell lines and bafilomycin for either LC3 (*F*(2,4) = 0.117, *p* = 0.89) or p62 (*F*(2,24) = 4.25, *p* = 0.0263). IP₃R, inositol triphosphate receptor; LC3, microtubule-associated protein light chain 3; MCU, mitochondrial Ca²⁺ uniporter.

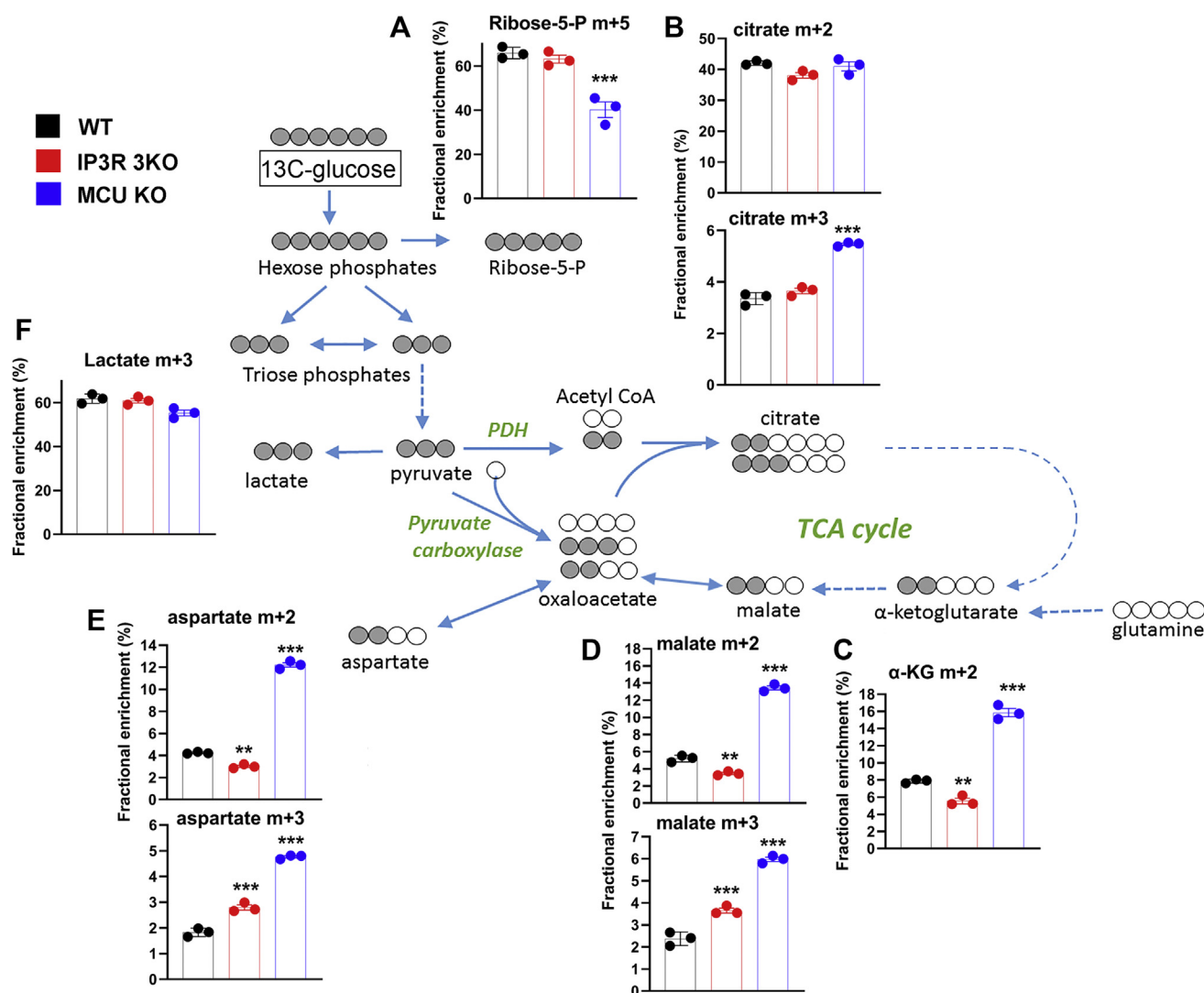


Figure 5. [U - ^{13}C]-glucose tracer analysis in WT, IP $_3$ R TKO, and MCU KO cells. Cells were incubated in glucose-free DMEM for 30 min, and then, the medium was replaced with DMEM containing 5 mM uniformly labeled ^{13}C -glucose for 5 or 60 min. Samples were prepared for LC-MS as described in the “Experimental procedures” section. Only the 60 min data for selected metabolites are shown in (A–F). Data are the fractional enrichment of the indicated isotopolog given as the mean \pm SEM of three separate plates for each condition. A simplified cartoon of the flow of labeled carbon (shaded gray) is shown with steps involving multiple enzymes being indicated by dotted arrows. * $p < 0.05$; ** $p < 0.01$; *** $p < 0.001$; **** $p < 0.0001$, one-way ANOVA followed by multiple comparison analysis using Dunnett’s test. DMEM, Dulbecco’s modified Eagle’s medium; IP $_3$ R, inositol trisphosphate receptor; MCU, mitochondrial Ca^{2+} uniporter; TKO, triple KO.

tracer experiments, the glucose in DMEM was reduced to 5 mM for 30 min and then switched to 5 mM U - ^{13}C -glucose for 5 and 60 min. We found the labeling of glycolytic intermediates to be the same at both time points, and therefore, only the 60 min data are shown (Fig. 5). The rapid labeling kinetics precluded any conclusions regarding differences in glycolytic rates based on U - ^{13}C -glucose experiments. The fractional enrichment (FE) of $m + 5$ ribose-5-phosphate was decreased in MCU KO cells suggesting that less glucose carbon may be diverted into the pentose phosphate shunt in these cells (Fig. 5A). This would be compatible with the measured increase in the NADP/NADPH ratio (Fig. S2A). The flow of glucose carbon into the TCA cycle was significantly slower than the labeling of glycolytic intermediates since negligible labeling of TCA cycle intermediates was observed at 5 min (not shown). Despite our observations on the differences in

phosphorylation state of PDH, the incorporation of two carbon units into citrate *via* PDH was not significantly different in the three cell lines (Fig. 5B). Whereas FE of $m + 2$ citrate reached $\sim 40\%$, the FE of $m + 2$ in α -KG (Fig. 5C), malate (Fig. 5D), or aspartate (a surrogate for labeling in oxaloacetate; Fig. 5E) was much lower in all three cell lines (3–15%). In part, this discrepancy could arise if substantial amounts of citrate are exported from the mitochondria to the cytosol for utilization in the ATP citrate lyase reaction that supplies acetyl CoA for lipid biosynthesis. The formation of $m + 2$ TCA metabolites was highest in the MCU KO cells (FE, 12–15%) indicating increased forward flux in the TCA cycle, which includes the segments containing Ca^{2+} -sensitive isocitrate and α -KG dehydrogenases.

The removal of TCA cycle intermediates for biosynthetic reactions necessitates anaplerotic pathways to replenish these

Metabolic adaptation to loss of calcium signaling

molecules. A major anaplerotic reaction involving glucose metabolism is the formation of oxaloacetate from pyruvate by the pyruvate carboxylase (PC) enzyme. This step acting on $m + 3$ pyruvate would generate $m + 3$ oxaloacetate which, in addition to being in equilibrium with $m + 3$ malate (Fig. 5D) and aspartate (Fig. 5E), can also generate $m + 3$ citrate (Fig. 5B). The formation of $m + 3$ citrate has been used to monitor PC flux in $U-^{13}C$ -glucose tracing experiments (59). In WT cells, PC flux was small (FE, ~3%) relative to the flux of carbon through PDH (FE, ~40%) (Fig. 5B). However, PC flux was selectively stimulated by ~70% in MCU KO cells (Fig. 5B).

Glutamine is a major substrate feeding carbon into the TCA cycle that can potentially supply both energy and biosynthetic intermediates (60). We therefore analyzed $U-^{13}C$ -glutamine metabolism in the three cell lines using time points of 30 min and 1 h. The sum of label accumulating in several glutamine metabolites (glutamate, α -KG, aspartate, citrate/isocitrate, and *cis*-aconitate) was taken as a measure of overall glutamine metabolism. This was found to be substantially increased in the MCU KO cells with a much smaller (but significant) increase also noted in the IP₃R 3KO cells (Fig. 6A). Metabolism of $U-^{13}C$ -glutamine by the combined actions of glutaminase,

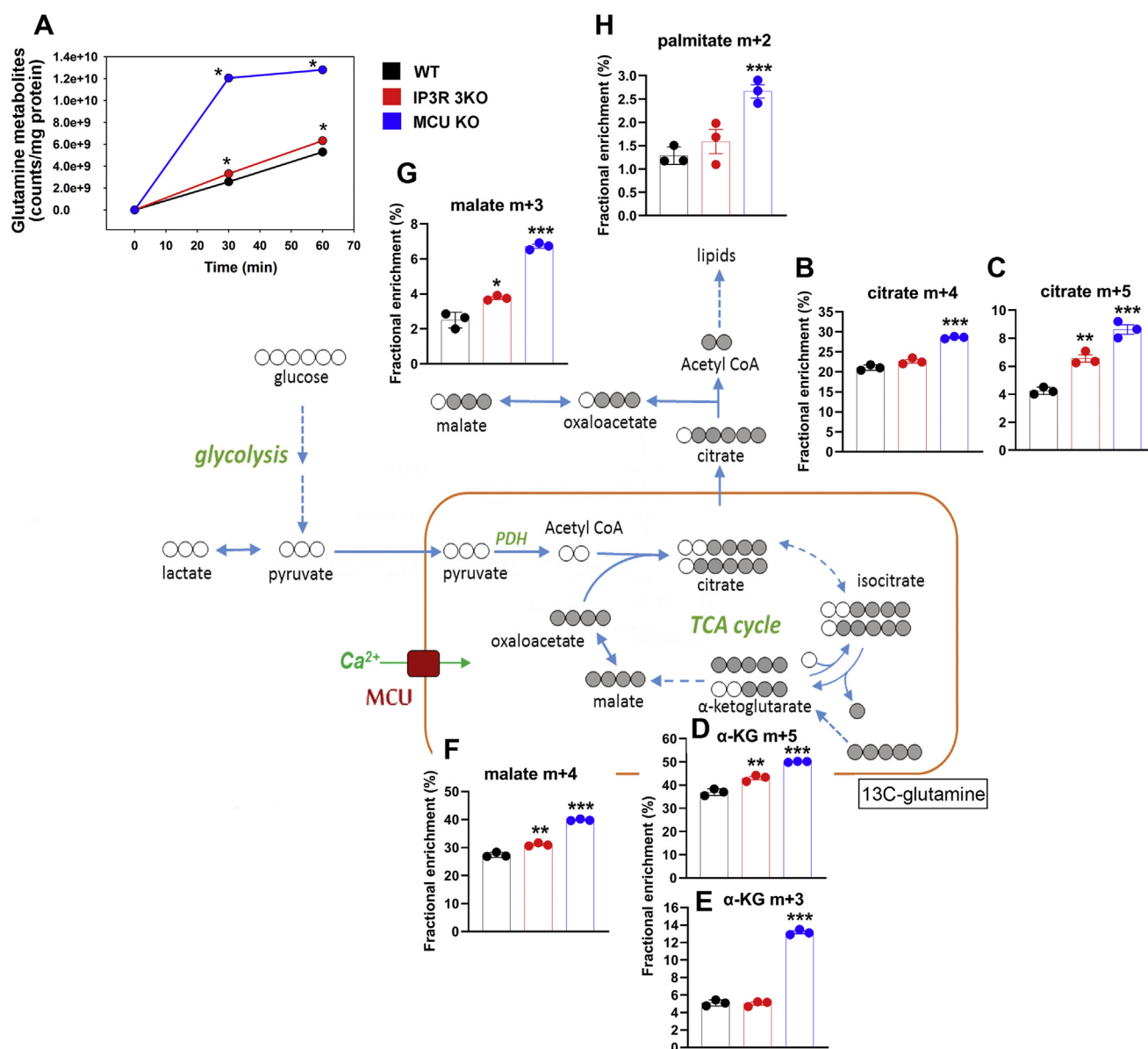


Figure 6. [$U-^{13}C$]-glutamine tracer analysis WT, IP₃R TKO, and MCU KO cells. Cells were washed in glutamine-free DMEM and then incubated in a DMEM containing 5 mM uniformly labeled ^{13}C -glutamine for 30 or 60 min. Samples were prepared for LC-MS/MS as described in the “Experimental procedures” section. A, the sum of counts appearing as glutamate, α -ketoglutarate, aspartate, citrate/isocitrate, and *cis*-aconitate was taken as a measure of glutamine metabolism. The data were normalized to protein. The error bars were smaller than symbol size. Only the 60 min data for selected metabolites are shown in (B–H). Data are the fractional enrichment of the indicated isotopolog given as the mean \pm SEM of three separate plates for each condition. A simplified cartoon of the flow of labeled carbon (shaded gray) is shown with steps involving multiple enzymes being indicated by dotted arrows. * $p < 0.05$; ** $p < 0.01$; *** $p < 0.001$; **** $p < 0.0001$, one-way ANOVA followed by multiple comparison analysis using Dunnett’s test. DMEM, Dulbecco’s modified Eagle’s medium; IP₃R, inositol triphosphate receptor; MCU, mitochondrial Ca²⁺ uniporter; TKO, triple KO.

glutamate dehydrogenase, and glutamate transaminases would generate $m + 5$ labeled α -KG. The “forward” direction of the TCA cycle would generate $m + 4$ oxaloacetate, and condensation with unlabeled acetyl-CoA would produce $m + 4$ citrate. Any limitation in the supply of acetyl-CoA as a result of a block at PDH should lower labeling of $m + 4$ citrate, but this was not observed for either of the KO cell lines (Fig. 6B). Indeed, a small increase was seen in the MCU KO cells. The same pattern of changes was also seen for $m + 4$ labeled malate (Fig. 6F), indicating no suppression of flux at the Ca^{2+} -sensitive α -KG dehydrogenase step. As observed in the glucose labeling data, the oxidative flux through the citrate/ α -KG span is increased in the MCU KO cells (Fig. 6E). Carbon entering the TCA cycle as α -KG can also proceed in the “reverse” direction as a result of reductive carboxylation (RC) to generate $m + 5$ labeled isocitrate, which is in equilibrium with citrate (Fig. 6C). This reverse flux in WT cells was $\sim 20\%$ of the oxidative flux as judged by the relative FEs of $m + 4$ and $m + 5$ citrates (Fig. 6, B and C). In IP_3R TKO cells, this ratio of fluxes was increased to $\sim 30\%$. In MCU KO cells, there was a twofold increase in RC flux, but since the oxidative flux was also increased, the overall

partitioning of the two pathways was also $\sim 30\%$. There is evidence that RC of glutamine can supply acetyl-CoA for fatty acid biosynthesis *via* mitochondrial citrate export and cleavage by the ATP-citrate lyase reaction (61–63). This reaction acting on $m + 5$ citrate would generate $m + 3$ malate (a proxy for $m + 3$ oxaloacetate). Indeed, the labeling of $m + 3$ malate in the three cell lines follows the same pattern as $m + 5$ citrate (Fig. 6G). MCU KO cells showed a significantly increased labeling of $m + 2$ palmitic acid by acetyl-CoA derived from glutamine metabolism (Fig. 6H).

KO HeLa cells and MCU rescue of HEK293T cells

To determine if the observed phenotypes of the IP_3R TKO and MCU KO are unique to HEK293 cell lines, we examined the effects of these KOs in the HeLa cell line. The IP_3R TKO HeLa cells have been used previously and shown to completely lack histamine-induced cytosolic Ca^{2+} transients (32). CRISPR-mediated gene targeting was used to produce the MCU KO HeLa cells (Fig. 7A). Loss of MCU function in the KO cells was confirmed by the lack of uptake of a pulse of

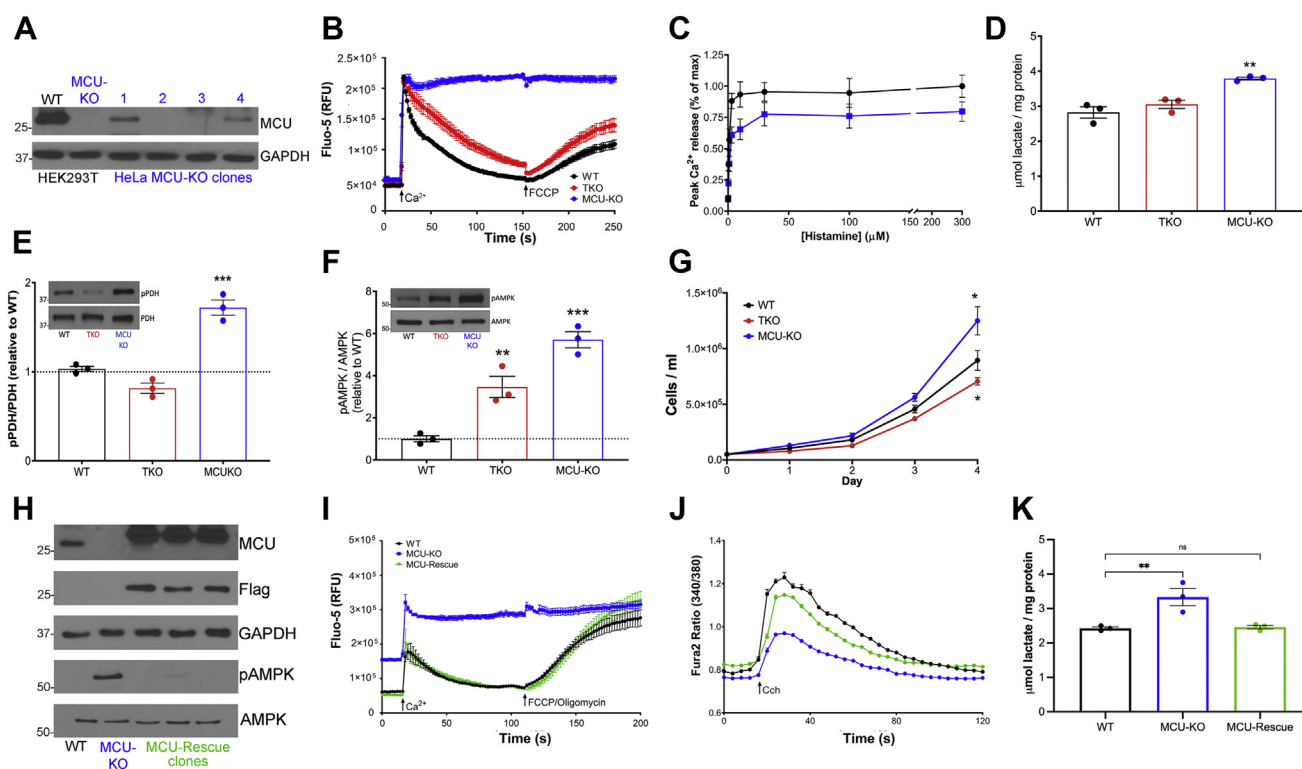


Figure 7. Characteristics of HeLa cells with IP_3R and MCU KOs and MCU-rescued HEK293T MCU KO cells. A, MCU immunoblotting confirmed loss of MCU in two of four HeLa clones after CRISPR KO. HEK293T WT and MCU-KO cells were used as positive and negative controls, respectively. GAPDH was the loading control. B, cells were permeabilized with saponin, and the clearance of a 50 μM pulse of Ca^{2+} added at 18 s was measured using Fluo-5 as described in the “Experimental procedures” section. A further addition of 1 μM FCCP was made as shown. C, HeLa cells were loaded with Fluo-8 AM as described in the “Experimental procedures” section, and changes to cytosolic Ca^{2+} in response to increasing doses of histamine were measured. D, neutralized PCA lysates of HeLa cells were assayed for lactate. Data are the mean \pm SEM, $n = 3$; $*p < 0.05$; $**p < 0.01$; $***p < 0.001$; $****p < 0.0001$, one-way ANOVA followed by multiple comparison analysis using Dunnett’s test. E and F, phosphorylation status of HeLa PDH and AMPK was measured by immunoblotting. Values are normalized to the total levels of each protein with each point representing the mean of an independent experiment performed in duplicate. G, growth curves for WT, TKO, and MCU-KO HeLa cell lines. Mean \pm SEM ($n = 3$). H, immunoblot for MCU and Flag in MCU-rescue in HEK293T clones. GAPDH was used as a loading control. The lower two panels show phosphorylated and total levels of AMPK. I, Ca^{2+} clearance in permeabilized HEK293T cells was measured as in (B). J, intact HEK293T cells were loaded with Fura-2 as described in the “Experimental procedures” section, and cytosolic Ca^{2+} changes in response to 25 μM carbachol was measured. K, lactate in HEK293T cells was measured in triplicate for three independent experiments as in (D). Statistical evaluation of data in (E–G) and (K) was as in (D). AMPK, AMP-dependent kinase; FCCP, (carbonylcyano-4-(trifluoromethoxy)phenyl)hydrazine; HEK293T, human embryonic kidney 293T cell line; IP_3R , inositol trisphosphate receptor; MCU, mitochondrial Ca^{2+} uniporter; PCA, perchloric acid; PDH, pyruvate dehydrogenase.

Metabolic adaptation to loss of calcium signaling

Ca²⁺ delivered to permeabilized HeLa cells (Fig. 7B). As noted previously (Fig. 1A), the MCU KO HEK293T cells display a smaller cytosolic Ca²⁺ response to a saturating dose of Cch. The MCU KO HeLa cells also gave a reduced response to histamine (Fig. 7C) when compared with WT HeLa cells, but the differences were smaller than noted in HEK293 cells. As observed in HEK293T cells, lactate levels were also elevated in MCU KO HeLa cells and were unchanged in IP₃R TKO cells (Fig. 7D). The smaller effects in HeLa cells may be related to their lesser reliance on glycolysis for ATP production than HEK293 cells (64, 65). The phosphorylation state of PDH (Fig. 7E), AMPK (Fig. 7F), as well as the growth rates of the different HeLa cell lines (Fig. 7G) were all qualitatively similar to the changes observed for the HEK293 cell lines. These data indicate that the observed phenotypes of MCU KO and IP₃R TKO cells are not unique to the HEK293 cell line.

Another concern of using KO cells is the possibility that the observed phenotypes are due to off-target effects of the knockdown methodology. To determine if this may be the case in the MCU KO HEK293T cells, we sought to determine if stably reintroducing the MCU reverted some of the observed changes. The rescued expression of MCU was confirmed by immunoblotting (Fig. 7H). The restoration of mitochondrial Ca²⁺ uptake could be demonstrated in Ca²⁺ clearance assays using permeabilized cells (Fig. 7I). In intact cells, the Cch-induced cytosolic Ca²⁺ increase was enhanced in the MCU-rescue cells when compared with the MCU KO cells and was approximately 85% of WT cells (Fig. 7J). The increased lactate levels (Fig. 7K) and increased AMPK phosphorylation (Fig. 7H, lower two panels) observed in MCU KO cells were also diminished toward levels observed in WT cells. We conclude that, at least for the parameters measured, the observed phenotype of MCU KO cells is unlikely to be due to off-target effects.

Forced utilization of the TCA cycle for energy production in the three cell lines

Constitutive Ca²⁺-stimulated mitochondrial oxidative metabolism has been proposed to be particularly important for maintaining the bioenergetics requirements of cancer cells (27, 28). This hypothesis is difficult to test in our KO models because HEK293 cells rely almost entirely on glycolysis to support their energy requirements (66, 67). Galactose metabolism minimizes the energy yield from glycolysis and makes cells increasingly reliant on the TCA cycle and oxidative phosphorylation to supply their energy needs (68). We therefore removed the glucose in DMEM and replaced it with 10 mM galactose. Oligomycin treatment of WT, IP₃R TKO, or MCU KO cells grown in glucose-containing medium had negligible effects on ATP levels, as expected if oxidative phosphorylation makes a minimal contribution to ATP production (Fig. 8A). By contrast, blocking glycolysis with iodoacetate lowered ATP levels in all three cell lines. Oligomycin markedly reduced ATP levels in all three cell lines incubated in galactose medium,

indicating the dominant role of oxidative phosphorylation under these conditions. The ability of the cell lines to maintain their levels of ATP and AMP was followed for different periods after the galactose switch. Over a period of 2 h, the cells had no difficulty in maintaining their ATP and AMP (Fig. 8, B and C). However, more prolonged incubation in galactose led to a progressive decrease in ATP and elevation of AMP in the MCU KO cells but not in the WT or IP₃R TKO cell lines. When cytotoxicity was measured with a fluorescent dye assay, it was evident that the MCU KO showed evidence of cell death that was significant at 18 h and markedly pronounced at 24 h after galactose incubation (Fig. 8D). There was no evidence of significant cytotoxicity in the WT or IP₃R TKO cell lines after prolonged incubation in galactose medium. Interestingly, the cytotoxicity observed in the MCU KO cells was strongly suppressed in the MCU-rescue cell line.

Discussion

The KO cell models used in this study were intended to compare the chronic metabolic and bioenergetic changes resulting from the loss of either cytosolic Ca²⁺ signaling (IP₃R TKO) and/or mitochondrial Ca²⁺ signaling (MCU KO and IP₃R TKO). The changes we measured are summarized in the scheme shown in Figure 9. The most prominent changes observed in the MCU KO HEK293T cells were increased glycolysis, glutamine metabolism, and increased growth rate. Presumably, the enhanced consumption of fuels and the increased oxygen consumption of MCU KO cell are needed to meet the demands of increased growth. Varied results have been reported when examining the effects of MCU loss on growth. Although we found an increased growth rate of MCU KO HEK293T and HeLa cells, Hall *et al.* (42) found HeLa cell proliferation to be decreased not only when MCU levels were diminished with siRNA but also when MCU activity was increased with MICU1 siRNA. Growth was diminished in MCU KO MEFs (47) but unaltered in siRNA-treated MD-MB-231 breast carcinoma cells (42). In agreement with our findings, knockdown of MCU in primary B lymphocytes enhanced proliferation in response to anti-immunoglobulin M (69).

A stimulation of glycolysis has been noted in several mouse models of MCU KO (34, 55) and MCU KO MEFs (47). The usual explanation offered for this effect is that loss of mitochondrial Ca²⁺ increases the phosphorylation state of PDH, and therefore diminishes its activity, which diverts pyruvate into lactate formation instead of entry into the TCA cycle. Although there are exceptions (39, 53), the loss of MCU is consistently associated with increased p-PDH (34, 50, 55, 56), as also seen in our MCU KO cells (Figs. 3F and 7F). However, there are several reasons for believing that lowered mitochondrial Ca²⁺ and p-PDH changes are not the underlying reason for the increased glycolysis. First, the mitochondrial Ca²⁺ content of WT and KO cells is already very low and can be estimated to be much lower than the *K_d* of the GEM-GECO probe (*i.e.*, <300 nM). Since the *K_{0.5}* for PDH activation by Ca²⁺ in isolated mitochondria is in the range of 300 to 500 nM

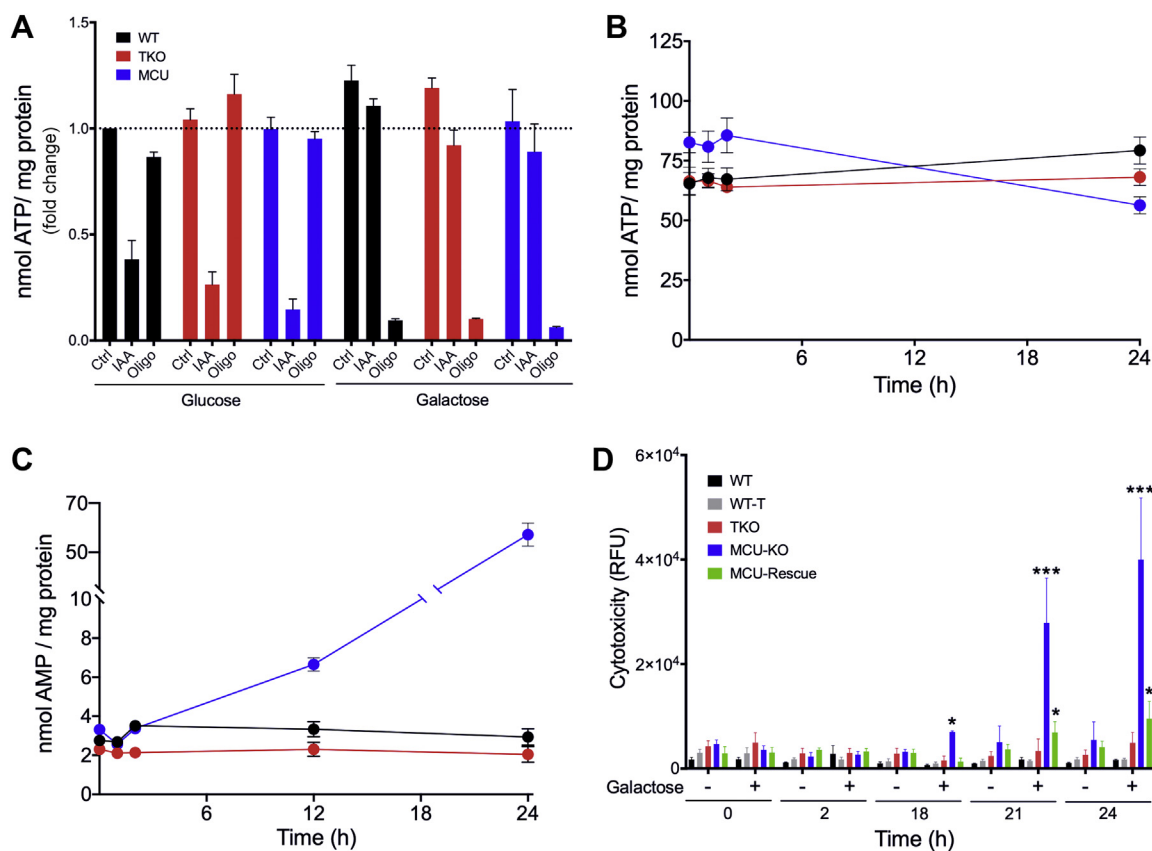


Figure 8. Forced utilization of the TCA cycle in HEK293 cells. A, 1.0×10^5 cells were seeded on 60 mm plates and grown for 72 h in glucose containing DMEM. Media were aspirated and replaced with glucose-free DMEM containing 10 mM galactose. Cells were treated with either 1 μ M iodoacetate (IAA) or 5 μ M oligomycin. After 1 h, cells were deproteinized in 0.6 M perchloric acid, neutralized, and ATP was measured with a luciferase assay. B–D, ATP, AMP, and cytotoxicity were measured at various time points following glucose removal and galactose addition. Values shown are the mean \pm SEM of three experiments. B, ATP was measured in neutralized PCA lysates using a luciferase assay. C, AMP was measured in neutralized PCA lysates using a Promega AMP-Glo assay. D, cell death was measured in real time using a Promega CellTox Green cytotoxicity assay, $n = 3$; * $p < 0.05$; ** $p < 0.01$; *** $p < 0.001$; **** $p < 0.0001$, two-way ANOVA followed by multiple comparison analysis using Dunnett's test. The data indicated a statistically significant interaction between the effects of cell lines and galactose ($F(28, 264) = 39.24$, $p < 0.0001$). DMEM, Dulbecco's modified Eagle's medium; HEK293, human embryonic kidney 293 cell line; PCA, perchloric acid; TCA, tricarboxylic acid.

(70), the small changes in baseline Ca^{2+} content are unlikely to have a major impact on levels of p-PDH. Second, only the MCU KO cells show substantially increased PDH phosphorylation, although both MCU KO and IP_3R TKO cells have comparable mitochondrial Ca^{2+} signals. Previous studies in intact mitochondria have shown that the stimulatory effects of Ca^{2+} on PDH phosphatase are more evident when the activity of PDH kinase is partially inhibited (71). Pyruvate and NADH are both regulators of PDH kinase and their changes in MCU KO cells are in the direction that would act to partially inhibit PDH kinase (72). Since these metabolites do not change in IP_3R TKO cells, it is possible that the sensitivity of PDH has shifted to a lower range of mitochondrial Ca^{2+} content in MCU KO cells. Finally, the direct measurement of isotope tracer flux of $[\text{U}-^{13}\text{C}]$ glucose carbon into $m + 2$ citrate showed no significant differences between the cell lines, indicating that the flow of carbon into the TCA cycle was not diminished despite increased p-PDH. A similar finding was made in a mouse heart MCU KO model using NMR to study the metabolism of $[\text{U}-^{13}\text{C}]$ glucose (73). The increased levels of the PDH substrate pyruvate in the MCU KO cells probably

contributes to the maintenance of PDH flux, despite enhanced PDH phosphorylation. If PDH flux is not the critical factor then what else could account for enhanced glycolysis in MCU KO cells? Flux through glycolysis is affected by multiple regulatory mechanisms, but one key factor is the cytosolic NAD^+/NADH ratio, which modulates the activity of glyceraldehyde 3-phosphate dehydrogenase. A continuous supply of NAD^+ to this enzyme is maintained by NADH utilization by the NADH oxidases of the respiratory chain and enzymes such as LDH and malate dehydrogenase in the cytosol. MCU KO cells have an increased NAD^+/NADH ratio that is mainly because of a fall in NADH levels (Fig. 2). Both basal respiration and lactate formation are increased in MCU KO cells. Elevated NAD^+/NADH ratios with decreased NADH levels has been shown to enhance glycolytic rate in several experimental systems (74–77). An additional factor that may contribute to enhanced glycolysis in MCU KO cells is the activation of AMPK (Fig. 3E), which is known to phosphorylate and stimulate phosphofructokinase-2 (78).

Maintaining the higher growth rate of MCU KO cells requires an increased supply of both energy and biosynthetic

Metabolic adaptation to loss of calcium signaling

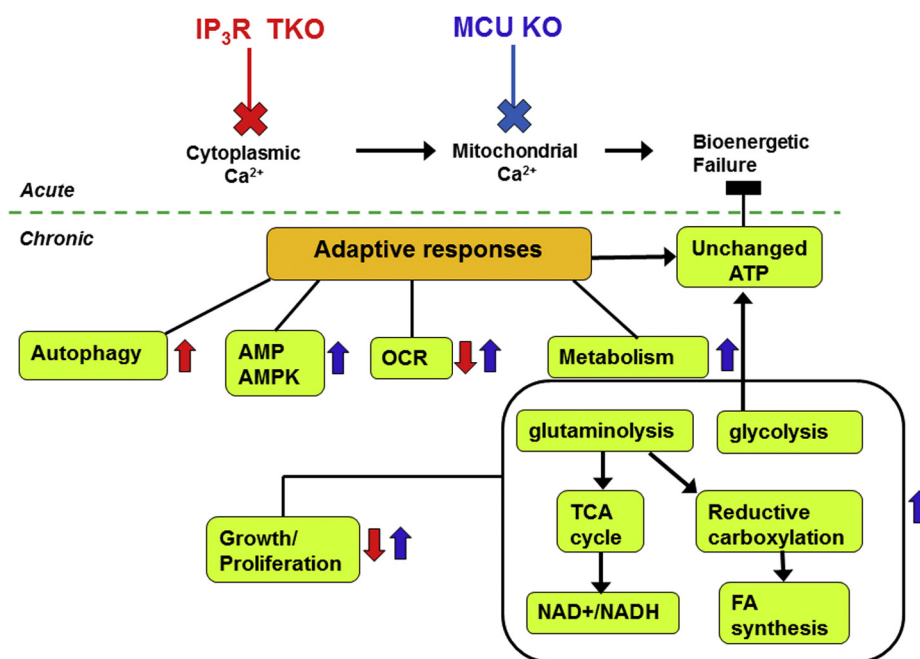


Figure 9. Schematic summarizing some of the pathways altered by the chronic loss of IP₃Rs and MCU. The acute responses to loss of ER–mitochondrial Ca²⁺ transport in cancer cells as documented in the literature (29, 30, 94) are shown above the dotted line. The adaptive chronic changes measured in the present study are shown below the dotted line. Upregulated or downregulated parameters are indicated by arrows colored red for IP₃R TKO and blue for MCU KO. The absence of an arrow indicates no change or minimal change in that parameter. Unlike acute effects, the chronic loss of ER–mitochondrial Ca²⁺ signaling maintains ATP levels and avoids bioenergetic failure. ER, endoplasmic reticulum; IP₃R, inositol trisphosphate receptor; MCU, mitochondrial Ca²⁺ uniporter.

building blocks. It is well established that glutamine metabolism contributes to both functions (79), and enhanced glutamine metabolism often accompanies increased aerobic glycolysis in cancer cells (60). Stimulated glutamine metabolism has been reported in MCU KO fibroblasts (47). Our experiments with [U-¹³C] glutamine show that MCU KO HEK293T cells have an increased flow of glutamine carbon into the TCA cycle, and the metabolism of α -KG is enhanced in both the oxidative and reductive directions (Fig. 6). The increased flux in the oxidative direction occurs independently of any increase in mitochondrial Ca²⁺ and may be related to the increased citrate (Fig. S2B) and lowered NAD(P)H (Figs. 2G and S2A), both of which are allosteric modifiers of mitochondrial isocitrate dehydrogenase-3. Increased flux of α -KG in the oxidative pathway is also required to supply the reducing equivalents required for RC (80). RC is commonly observed in the absence of an adequate supply of acetyl-CoA from PDH, as seen, for example, in hypoxia (81). Since PDH flux is not altered in MCU KO cells, the stimulated RC is more likely to be secondary to increased α -KG availability provided by enhanced glutamine metabolism. Interestingly, increased RC also accompanies stimulated glycolysis (82, 83) or high extracellular lactate (84). Both these conditions prevail in MCU KO cells. A further important conclusion from the ¹³C-tracer studies is the lack of suppression of basal flux through any of the three Ca²⁺-sensitive TCA cycle dehydrogenases when MCU or IP₃Rs are deleted, implying that any small decreases in basal mitochondrial [Ca²⁺] occurring in the KO cells are not sufficient to impact flux through these enzymes. This conclusion contrasts with the recent findings of

Cardenas *et al.* (29) that constitutive Ca²⁺ regulation of α -KG dehydrogenase is required to maintain RC in a mutant osteosarcoma cell line with defective oxidative phosphorylation.

The main changes observed in IP₃R TKO HEK293 cells were a reduced growth rate, reduced oxygen consumption, and an increased basal rate of autophagy with no changes in glucose or glutamine consumption. Some of these observations are in agreement with previous studies. A lower rate of proliferation and migration in IP₃R TKO HEK293 cells has been reported recently (31). A reduced baseline and FCCP-stimulated oxygen consumption was observed in Seahorse assays (85). Acute inhibition or chronic loss of IP₃Rs promotes an increase in basal autophagy in several cell types, but different mechanisms for this effect have been proposed (86, 87). In our studies, it is clear that the effects are independent of AMPK activation. Only minor changes in metabolic rewiring could be observed in the ¹³C-tracer studies, including an increase in anaplerosis of glucose carbon through PC, and an increase in RC of glutamine and palmitate syntheses. All these effects were significantly smaller than observed with MCU KO cells (Figs. 5 and 6). Overall, the data show that the loss of mitochondrial Ca²⁺ signaling induced by the stable KO of IP₃Rs or MCU produce quite distinct phenotypes. We cannot exclude the possibility that some of the changes seen in MCU KO cells may result from the loss of a scaffolding role of the MCU protein itself, rather than the lack of mitochondrial Ca²⁺ fluxes. Further investigation of the protein–protein interactions of MCU in the mitochondrial matrix and the role of these complexes in regulating the structure/function of mitochondria are required to test this

possibility. Electron microscopy images of MCU KO HEK293T cells provided no indication of differences in gross mitochondrial structure or ER/mitochondrial distances (not shown). Both HEK293T and HeLa cells show a decreased agonist-mediated cytosolic Ca^{2+} response in the MCU KO cells (Figs. 1, A and H, and 7C). However, an increased agonist-mediated Ca^{2+} transient has been reported in other MCU KO models including MEFs (47) and vascular smooth muscle cells (46), where the result has been attributed to a lack of mitochondrial Ca^{2+} buffering. The intracellular store Ca^{2+} content or the dynamics of IP_3 -mediated Ca^{2+} puffs were not altered in MCU KO HEK293 cells (69). Thus, mechanisms acting upstream of IP_3 synthesis/degradation, or affecting Ca^{2+} extrusion from the cytosol *via* plasma membrane or ER Ca^{2+} pumps, are more likely to be involved. Increased rates of both ER and plasma membrane Ca^{2+} pumping have been reported in several MCU KO cell types (69). Further studies are required to establish a definitive mechanism for the decreased cytosolic Ca^{2+} signaling observed in our MCU KO cells.

A hypothesis that has gained general acceptance is that the baseline bioenergetic needs of both normal and cancer cells requires constitutive ER-to-mitochondrial Ca^{2+} translocation in order to stimulate mitochondrial Ca^{2+} -dependent dehydrogenases of the TCA cycle (27, 28). It is argued that cancer cells are particularly “addicted” to this process, which, if interrupted, limits ATP supply for cell division and results in cell death (27–29). The main evidence for this hypothesis has been acquired primarily after acute treatment with the drug Xestospingon-B (which targets the IP_3R) and siRNA silencing of MCU or IP_3R (27, 28). Our experimental conditions differ because we have examined the long-term effects of MCU and IP_3R gene disruption. The studies show that these cells have adapted to maintain their ATP levels, with no requirement for basal mitochondrial or cytosolic Ca^{2+} signaling. This suggests that glycolysis has adequate excess capacity to maintain ATP requirements and that sufficient mitochondrial Ca^{2+} is present to operate the TCA cycle and supply biosynthetic precursors. This appears to be true even when glycolysis and glutamine metabolism are accelerated to accommodate the increased growth rate of MCU KO cells. However, differences in behavior are revealed when the cells are switched from glucose to galactose so that they predominantly rely on the TCA cycle for both energy and biosynthetic precursors. Under these conditions, the MCU KO cells show evidence of bioenergetic failure with ATP loss, AMP accumulation, and cell death (Fig. 9). This phenotype is suppressed in the MCU-rescue cells. Surprisingly, the IP_3R TKO cells are unaffected by the galactose switch, again underscoring that basal metabolism is relatively insensitive to Ca^{2+} in these cells. A cell death assay using a 24 h period of incubation of K562 leukemic cells in galactose has been used to screen for genes involved in oxidative phosphorylation (88). Further studies are needed to determine if the behavior of the MCU KO cells in galactose medium simply reflects the inability to meet ATP demand (*e.g.*, for mitosis), or if there are secondary defects in the oxidative phosphorylation machinery.

Calcium is viewed as a universal second messenger regulating a wide variety of biological processes (1). Global and conditional mouse KO of IP_3R isoforms have supported a biologically important role for intracellular Ca^{2+} signals (15). Yet, it is also apparent that several cancer cells (*e.g.*, HEK293, HeLa, and DT40 lymphocytes) can survive the loss of all three IP_3R isoforms. Several evolutionary lineages either lack recognizable IP_3Rs (89, 90) or have independently lost IP_3Rs while retaining MCU homologs (91, 92). Thus, the phenotype of cells without Ca^{2+} signaling may utilize ancestral Ca^{2+} -independent signaling mechanisms and/or additional transcriptional rewiring resulting from disruption of IP_3R genes. Future RNA-Seq studies could provide useful information on the molecular mechanisms underlying the adaptive responses of growth and metabolism seen after loss of IP_3Rs and MCU. Targeting Ca^{2+} signaling with drugs that block ER–mitochondrial communication is being explored as a strategy for the treatment of various diseases where there is aberrant translocation of Ca^{2+} into the mitochondria (93–95). Chronic use of these drugs may induce metabolic and bioenergetic adaptations similar to those seen in the present study. Understanding these mechanisms would aid in optimizing the therapeutic benefits of blocking Ca^{2+} signaling in disease states.

Experimental procedures

Cell lines and culture

All cells were cultured at 37 °C and 5% CO_2 in DMEM supplemented with 5% fetal bovine serum, 1% penicillin/streptomycin, and 0.25 $\mu\text{g}/\text{ml}$ amphotericin B. HEK293 IP_3R TKO cells and HeLa IP_3R TKO cells were made as described previously (30, 32). Most of the experiments in this study used HEK293T MCU KO cells made by TALEN knockdown that were obtained from the laboratory of Dr Vamsi Mootha (48). The appropriate controls for the IP_3R TKO and MCU KO cells are WT HEK293 cells and HEK293T cells, respectively. We have compared several parameters investigated in the present study and did not find them to be significantly different in the controls (Figs. 1A and 2A and S1). Therefore, the main figures show only the WT HEK293 cells as the controls for both IP_3R TKO and MCU KO cells.

Ca^{2+} measurements

Trypsin-released cells were seeded on a black, clear-bottom, and 96-well plate at a density of 5×10^5 cells/well and incubated at 37 °C and 5% CO_2 for 24 h. Media were aspirated from all wells of the plate and replaced with 190 μl of Ca^{2+} -assay buffer (Hank’s balanced salt solution containing MgCl_2 [1 mM], CaCl_2 [2.3 mM], and 20 mM Hepes [pH 7.2]) supplemented with 5 μM Fluo8-AM, 500 μM Brilliant Black, and 100 μM sulfinpyrazone. The plate was maintained in the incubator for 45 min. Changes in cytosolic Ca^{2+} were monitored using a FlexStation II plate reader in fluorescence mode at 37 °C. Measurements were made using excitation and emission wavelengths of 485 and 525 nm, respectively. The additions of Cch, FCCP, oligomycin, and ionomycin were

Metabolic adaptation to loss of calcium signaling

made by utilizing the automated fluidics system of the hardware. In some experiments, cells were loaded as aforementioned with 1 μM Fura2-AM, and Ca^{2+} was measured ratiometrically using excitation and emission wavelengths of 340/380 and 510 nm, respectively. Ca^{2+} fluxes in permeabilized cells were measured after harvesting cells grown in 100 mm plates with trypsin. The cells were centrifuged (1000g; 2 min), washed in $\text{Ca}^{2+}/\text{Mg}^{2+}$ -free Hank's balanced salt solution and then resuspended in 600 μl of dye buffer (2 μM Fluo-5N, 120 mM KCl, 1 mM MgCl_2 , 25 mM Hepes [pH 7.2], 5 mM succinate, 2 mM TrisPi, 4 μM rotenone, and 1 μM thapsigargin), and permeabilized using saponin (10 μg). Permeabilization was verified by trypan blue staining. Aliquots (90 μl) were transferred to wells of a black transparent bottom 96-well plate. The plate was maintained at 37 $^\circ\text{C}$, and measurements were made using excitation and emission wavelengths of 491 and 516 nm, respectively.

For imaging experiments, cells were preincubated in a serum-free extracellular medium (121 mM NaCl, 5 mM NaHCO_3 , 10 mM Na-Hepes, 4.7 mM KCl, 1.2 mM KH_2PO_4 , 1.2 mM MgSO_4 , 2 mM CaCl_2 , and 10 mM glucose [pH 7.4]) containing 2% bovine serum albumin (BSA). For measurements of $[\text{Ca}^{2+}]_c$, cells were loaded with 2 μM Cal520-AM (AAT Bioquest) together with 0.003% pluronic F127 and 100 μM sulfinpyrazone for 30 min at 30 $^\circ\text{C}$. At the end of the preincubation or dye-loading period, the cells were washed into fresh extracellular medium containing 0.25% BSA and transferred to the temperature-regulated stage (37 $^\circ\text{C}$) of the microscope. Fluorescence wide-field imaging of $[\text{Ca}^{2+}]_c$ and $[\text{Ca}^{2+}]_m$ was carried out using a back-illuminated electron multiplying charge-coupled device camera (Photometrics). GEM-GECO was excited with 403/10 nm, whereas emission pairs were monitored using 435/30 nm (Ca^{2+} -free) and 550/30 nm (Ca^{2+} -bound) emission filters. Cal520 was imaged using 490/10 nm excitation filters and a 550 nm long-pass beam splitter, and an image triplet was obtained every 250 ms to maximize kinetic information. Fluorescence is presented as F/F_0 or GEM-GECO emission ratios, calculated following background subtraction of the individual wavelengths.

Growth curves

About 2.5×10^5 HEK293, HEK293T, or HeLa cell lines were plated on 100 mm plates. At the indicated times, plates were trypsinized for 4 min and resuspended in 10 ml DMEM. The cell density was counted in triplicate using a hemocytometer.

Metabolite assays

Glucose consumption was measured after a 1 h period in which the cells were incubated in glucose-free medium. About 5 mM glucose was then added, and aliquots of the media (250 μl) were removed for glucose assay at the indicated times. A previously described colorimetric method using glucose oxidase was modified for use on a plate reader as described (96). Lactate was measured in neutralized perchloric acid (PCA) lysates using LDH as previously described (97). Pyruvate was measured with pyruvate oxidase and Amplex red (98).

Nicotinamide nucleotides were measured using enzymatic cycling assays. Cells grown on 10 cm^2 plates were released with 0.25% trypsin/EDTA and centrifuged (1000g; 5 min). The pellets were resuspended in 1 ml PBS, split into two equal aliquots, and recentrifuged. For $\text{NAD}^+/\text{NADP}^+$ assay, the cell pellet was resuspended with 100 μl 0.6 M PCA. For NADH/NADPH assay, the cell pellet was resuspended in 100 μl of 1 M KOH, heated at 65 $^\circ\text{C}$ for 30 min, and briefly sonicated (10 s). All samples were stored at -80°C prior to assay. NAD^+ and NADH were measured by an enzymatic cycling assay using alcohol dehydrogenase (99). NADP^+ and NADPH were measured by an enzymatic cycling assay using glucose-6-phosphate dehydrogenase (100). ATP was assayed in neutralized PCA extracts using a luciferase method (101). AMP was assayed using the AMP-glo kit (Promega) following the manufacturer's instructions.

SDS-PAGE/Western blotting

To prepare lysates, cells incubated in DMEM were washed in PBS and lysed in a medium (0.250 ml) containing 1% Triton X-100, 50 mM Tris-HCl (pH 7.8), 150 mM NaCl, 2 mM sodium orthovanadate, 10 mM sodium pyrophosphate, 20 mM NaF, and a 1 \times dilution of a complete protease inhibitor mixture (Roche Diagnostics). The lysates were centrifuged at 12,000g for 10 min. The supernatants were denatured in SDS sample buffer. Lysates were boiled at 100 $^\circ\text{C}$ for 5 min and then stored at -20°C until use. Unless otherwise noted, 40 μg of protein were run at 100 V for 90 min on 10% polyacrylamide gels and transferred at 100 V for 60 min onto nitrocellulose membranes. Polyvinylidene difluoride membranes were used in the specific case of LC3 immunoblotting. Membranes were blocked in Tris-buffered saline with Tween-10 supplemented with 5% BSA for 1 h at room temperature. Following 3 \times 15 min washes in Tris-buffered saline with Tween-10, the primary antibody was added for 16 h at 4 $^\circ\text{C}$. All the antibodies were used at a dilution of 1:1000 and were obtained from Cell Signaling. Membranes were developed using ECL reagent (Thermo Fisher Scientific). When necessary, membranes were stripped using a buffer containing SDS (2%; w/v), Tris (62.5 mM; pH 6.8), and β -mercaptoethanol (100 mM).

Oxygen consumption

Cells were seeded at a density of 2×10^5 and were grown on 60 mm plates for 5 days. Trypsinized cells (10^6) resuspended in DMEM were introduced into the chamber of an O_2 electrode (Oroboros Instruments GmbH). Baseline rates of O_2 consumption and the rates after sequential addition of 5 μM oligomycin, 10 μM FCCP, and 1 μM antimycin A were measured.

Labeled isotope tracing

Cells were seeded on 60 mm plates with 2×10^5 cells in DMEM and grown for 5 days. To label with glutamine, the DMEM, containing all other components except glutamine, was supplemented with 4 mM L -[U - ^{13}C] glutamine. The plates were labeled in triplicate with 1 ml of medium for

30 and 60 min. To label with glucose, the DMEM, containing all other components except glucose, was supplemented with 5 mM D-[U-¹³C] glucose. The plates were labeled in triplicate with 1 ml medium for 5 and 60 min. At the indicated times, the plates were aspirated and rapidly washed in ice-cold PBS. Metabolites were extracted by rocking in 0.5 ml buffer containing 5:3:2 ratios of methanol, acetonitrile, and water for 10 min at 4 °C. The solvent was removed, centrifuged at 12,000g for 10 min, and stored at -80 °C prior to analysis. LC-MS analysis was performed on a Q Exactive HybridQuadrupole-Orbitrap HF-X MS (Thermo Fisher Scientific) equipped with a HESI II probe and coupled to a Vanquish Horizon UHPLC system (Thermo Fisher Scientific). Conditions for chromatography, mass spectroscopy, identification, and quantitation of metabolites were as detailed in the study by Casciano *et al.* (102).

CRISPR-Cas9 MCU KO and rescue

MCU KO clones of HeLa cells were obtained using Cas9/guide RNA ribonucleoprotein complexes (103). Two CRISPR RNA sequences were used: GAUCGCUUCCUGGCAGAAUUGUUUUAGAGCUAUGCU; UGAACUGACAGCGUUCACGCGUUUUAGAGCUAUGCU. Guide RNA complexes were formed by annealing the CRISPR RNA with transactivating RNA as described by Jacobi *et al.* (104). The complexes were combined with recombinant Cas9 nuclease and transfected into HeLa cells with Lipofectamine 3000. RNAs and Cas9 were purchased from Integrated DNA Technologies. After 1 week of growth, the cells were subcloned by limiting dilution into 96-well plates. Individual clones were expanded into 35 mm plates and screened for MCU expression by immunoblotting. MCU rescue in MCU KO HEK293T cells was carried out by transfecting a plasmid encoding a C-terminal FLAG-tagged human MCU (Addgene; catalog no.: 50054) using Lipofectamine 3000 and selecting for stable transfectants using hygromycin (20 µg/ml).

Data collection and analysis

Unless otherwise noted, the data are expressed as means ± SEM of three independent experiments, each performed in technical triplicate. GraphPad Prism (GraphPad Software, Inc) was used to generate plots and perform statistical analysis. A complete list of statistical analysis of the figures can be found in Table S1.

Data availability

All data generated or analysed during this study are included in this published article (and its [supplementary information](#) files).

Supporting information—This article contains supporting information.

Acknowledgments—We thank Drs Sergio De La Fuente Perez and Mate Katona for helpful advice.

Author contributions—M. P. Y., D. I. Y., K. M., G. H., and S. K. J. conceptualization; D. M. B., D. I. Y., K. M., and S. K. J. methodology; M. P. Y., Z. T. S., D. M. B., D. I. Y., and G. H. formal analysis; D. I. Y., K. M., G. H., and S. K. J. resources; M. P. Y., Z. T. S., D. M. B., D. I. Y., G. H., and S. K. J. data curation; M. P. Y. and Z. T. S. writing—original draft; M. P. Y., D. I. Y., K. M., G. H., and S. K. J. writing—review and editing; M. P. Y. and S. K. J. project administration; M. P. Y., G. H., and S. K. J. funding acquisition.

Funding and additional information—This work was supported by the National Institutes of Health (NIH) RO1 grants GM132611 (to S. K. J.), GM102724 (to G. H.), and DE014756 (to D. I. Y.). Z. T. S. was supported by the NIH/National Cancer Institute CA249950 and CA114046. M. P. Y. and D. M. B. were supported by an NIH National Institute on Alcohol Abuse and Alcoholism training grant T32-AA007463. The content is solely the responsibility of the authors and does not necessarily represent the official views of the NIH.

Conflict of interest—The authors declare that they have no conflicts of interest with the contents of this article.

Abbreviations—The abbreviations used are: AMPK, AMP-dependent kinase; BSA, bovine serum albumin; Cch, carbachol; DMEM, Dulbecco's modified Eagle's medium; ER, endoplasmic reticulum; FCCP, (carbonylcyanide-4-(trifluoromethoxy)phenylhydrazone); FE, fractional enrichment; HEK293, human embryonic kidney 293 cell line; IP₃R, inositol trisphosphate receptor; α-KG, α-ketoglutarate; LC3, microtubule-associated protein light chain 3; LDH, lactate dehydrogenase; MCU, mitochondrial Ca²⁺ uniporter; MEF, mouse embryonic fibroblast; OCR, oxygen consumption rate; PC, pyruvate carboxylase; PCA, perchloric acid; PDH, pyruvate dehydrogenase; p-PDH, phosphorylated PDH; RC, reductive carboxylation; TCA, tricarboxylic acid; TKO, triple KO.

References

- Berridge, M. J. (1993) Inositol trisphosphate and calcium signalling. *Nature* **361**, 315–325
- Foskett, J. K., White, C., Cheung, K. H., and Mak, D. O. (2007) Inositol trisphosphate receptor Ca²⁺ release channels. *Physiol. Rev.* **87**, 593–658
- Mammucari, C., Gherardi, G., and Rizzuto, R. (2017) Structure, activity regulation, and role of the mitochondrial calcium uniporter in health and disease. *Front. Oncol.* **7**, 139
- Bagur, R., and Hajnoczky, G. (2017) Intracellular Ca(2+) sensing: Its role in calcium homeostasis and signaling. *Mol. Cell* **66**, 780–788
- Denton, R. M. (2009) Regulation of mitochondrial dehydrogenases by calcium ions. *Biochim. Biophys. Acta* **1787**, 1309–1316
- Murphy, A. N., Kelleher, J. K., and Fiskum, G. (1990) Submicromolar Ca²⁺ regulates phosphorylating respiration by normal rat liver and AS-30D hepatoma mitochondria by different mechanisms. *J. Biol. Chem.* **265**, 10527–10534
- Territo, P. R., Mootha, V. K., French, S. A., and Balaban, R. S. (2000) Ca²⁺ activation of heart mitochondrial oxidative phosphorylation: Role of the F(0)/F(1)-ATPase. *Am. J. Physiol. Cell Physiol.* **278**, C423–C435
- Giorgio, V., Guo, L., Bassot, C., Petronilli, V., and Bernardi, P. (2018) Calcium and regulation of the mitochondrial permeability transition. *Cell Calcium* **70**, 56–63
- Matsumoto, M., Nakagawa, T., Inoue, T., Nagata, E., Tanaka, K., Takano, H., Minowa, O., Kuno, J., Sakakibara, S., Yamada, M., Yonehima, H., Miyawaki, A., Fukuuchi, Y., Furuichi, T., Okano, H., *et al.* (1996) Ataxia and epileptic seizures in mice lacking type 1 inositol 1,4,5-trisphosphate receptor. *Nature* **379**, 168–171
- Hisatsune, C., Yasumatsu, K., Takahashi-Iwanaga, H., Ogawa, N., Kuroda, Y., Yoshida, R., Ninomiya, Y., and Mikoshiba, K. (2007) Abnormal

- taste perception in mice lacking the type 3 inositol 1,4,5-trisphosphate receptor. *J. Biol. Chem.* **282**, 37225–37231
11. Nakazawa, M., Uchida, K., Aramaki, M., Kodo, K., Yamagishi, C., Takahashi, T., Mikoshiba, K., and Yamagishi, H. (2011) Inositol 1,4,5-trisphosphate receptors are essential for the development of the second heart field. *J. Mol. Cell. Cardiol.* **51**, 58–66
 12. Wang, H., Jing, R., Trexler, C., Li, Y., Tang, H., Pan, Z., Zhu, S., Zhao, B., Fang, X., Liu, J., Chen, J., and Ouyang, K. (2019) Deletion of IP3R1 by Pdgfrb-Cre in mice results in intestinal pseudo-obstruction and lethality. *J. Gastroenterol.* **54**, 407–418
 13. Lin, Q., Zhao, G., Fang, X., Peng, X., Tang, H., Wang, H., Jing, R., Liu, J., Lederer, W. J., Chen, J., and Ouyang, K. (2016) IP3 receptors regulate vascular smooth muscle contractility and hypertension. *JCI Insight* **1**, e89402
 14. Lin, Q., Zhao, L., Jing, R., Trexler, C., Wang, H., Li, Y., Tang, H., Huang, F., Zhang, F., Fang, X., Liu, J., Jia, N., Chen, J., and Ouyang, K. (2019) Inositol 1,4,5-trisphosphate receptors in endothelial cells play an essential role in vasodilation and blood pressure regulation. *J. Am. Heart Assoc.* **8**, e011704
 15. Mikoshiba, K. (2011) Role of IP(3) receptor in development. *Cell Calcium* **49**, 331–340
 16. Futatsugi, A., Nakamura, T., Yamada, M. K., Ebisui, E., Nakamura, K., Uchida, K., Kitaguchi, T., Takahashi-Iwanaga, H., Noda, T., Aruga, J., and Mikoshiba, K. (2005) IP3 receptor types 2 and 3 mediate exocrine secretion underlying energy metabolism. *Science* **309**, 2232–2234
 17. Uchida, K., Aramaki, M., Nakazawa, M., Yamagishi, C., Makino, S., Fukuda, K., Nakamura, T., Takahashi, T., Mikoshiba, K., and Yamagishi, H. (2010) Gene knock-outs of inositol 1,4,5-trisphosphate receptors types 1 and 2 result in perturbation of cardiogenesis. *PLoS One* **5**, e12500
 18. Yang, F., Huang, L., Tso, A., Wang, H., Cui, L., Lin, L., Wang, X., Ren, M., Fang, X., Liu, J., Han, Z., Chen, J., and Ouyang, K. (2020) Inositol 1,4,5-trisphosphate receptors are essential for fetal-maternal connection and embryo viability. *PLoS Genet.* **16**, e1008739
 19. Uchida, K., Nakazawa, M., Yamagishi, C., Mikoshiba, K., and Yamagishi, H. (2016) Type 1 and 3 inositol trisphosphate receptors are required for extra-embryonic vascular development. *Developmental Biol.* **418**, 89–97
 20. Ouyang, K., Leandro Gomez-Amaro, R., Stachura, D. L., Tang, H., Peng, X., Fang, X., Traver, D., Evans, S. M., and Chen, J. (2014) Loss of IP3R-dependent Ca²⁺ signalling in thymocytes leads to aberrant development and acute lymphoblastic leukemia. *Nat. Commun.* **5**, 4814
 21. Tang, H., Wang, H., Lin, Q., Fan, F., Zhang, F., Peng, X., Fang, X., Liu, J., and Ouyang, K. (2017) Loss of IP3 receptor-mediated Ca(2+) release in mouse B cells results in abnormal B cell development and function. *J. Immunol.* **199**, 570–580
 22. Wang, Y. J., Huang, J., Liu, W., Kou, X., Tang, H., Wang, H., Yu, X., Gao, S., Ouyang, K., and Yang, H. T. (2017) IP3R-mediated Ca²⁺ signals govern hematopoietic and cardiac divergence of Flk1+ cells via the calcineurin-NFATc3-Etv2 pathway. *J. Mol. Cell. Biol.* **9**, 274–288
 23. Sugawara, H., Kurosaki, M., Takata, M., and Kurosaki, T. (1997) Genetic evidence for involvement of type 1, type 2 and type 3 inositol 1,4,5-trisphosphate receptors in signal transduction through the B-cell antigen receptor. *EMBO J.* **16**, 3078–3088
 24. Taylor, C. W., Rahman, T., Tovey, S. C., Dedos, S. G., Taylor, E. J., and Velamakanni, S. (2009) IP3 receptors: Some lessons from DT40 cells. *Immunol. Rev.* **231**, 23–44
 25. Wen, H., Xu, W. J., Jin, X., Oh, S., Phan, C. H., Song, J., Lee, S. K., and Park, S. (2015) The roles of IP3 receptor in energy metabolic pathways and reactive oxygen species homeostasis revealed by metabolomic and biochemical studies. *Biochim. Biophys. Acta* **1853**, 2937–2944
 26. Khan, M. T., and Joseph, S. K. (2010) Role of inositol trisphosphate receptors in autophagy in DT40 cells. *J. Biol. Chem.* **285**, 16912–16920
 27. Cardenas, C., Miller, R. A., Smith, I., Bui, T., Molgo, J., Muller, M., Vais, H., Cheung, K. H., Yang, J., Parker, I., Thompson, C. B., Birnbaum, M. J., Hallows, K. R., and Foskett, J. K. (2010) Essential regulation of cell bioenergetics by constitutive InsP3 receptor Ca²⁺ transfer to mitochondria. *Cell* **142**, 270–283
 28. Cardenas, C., Muller, M., McNeal, A., Lovy, A., Jana, F., Bustos, G., Urrea, F., Smith, N., Molgo, J., Diehl, J. A., Ridky, T. W., and Foskett, J. K. (2016) Selective vulnerability of cancer cells by inhibition of Ca(2+) transfer from endoplasmic reticulum to mitochondria. *Cell Rep.* **14**, 2313–2324
 29. Cardenas, C., Lovy, A., Silva-Pavez, E., Urrea, F., Mizzone, C., Ahumada-Castro, U., Bustos, G., Jana, F., Cruz, P., Farias, P., Mendoza, E., Huerta, H., Murgas, P., Hunter, M., Rios, M., et al. (2020) Cancer cells with defective oxidative phosphorylation require endoplasmic reticulum-to-mitochondria Ca(2+) transfer for survival. *Sci. Signal.* **13**, eaay1212
 30. Alzayady, K. J., Wang, L., Chandrasekhar, R., Wagner, L. E., 2nd, Van Petegem, F., and Yule, D. I. (2016) Defining the stoichiometry of inositol 1,4,5-trisphosphate binding required to initiate Ca²⁺ release. *Sci. Signal.* **9**, ra35
 31. Yue, L., Wang, L., Du, Y., Zhang, W., Hamada, K., Matsumoto, Y., Jin, X., Zhou, Y., Mikoshiba, K., Gill, D. L., Han, S., and Wang, Y. (2020) Type 3 inositol 1,4,5-trisphosphate receptor is a crucial regulator of calcium dynamics mediated by endoplasmic reticulum in HEK cells. *Cells* **9**, 275
 32. Ando, H., Hirose, M., and Mikoshiba, K. (2018) Aberrant IP3 receptor activities revealed by comprehensive analysis of pathological mutations causing spinocerebellar ataxia 29. *Proc. Natl. Acad. Sci. U. S. A.* **115**, 12259–12264
 33. Garbincius, J. F., Luongo, T. S., and Elrod, J. W. (2020) The debate continues - what is the role of MCU and mitochondrial calcium uptake in the heart? *J. Mol. Cell. Cardiol.* **143**, 163–174
 34. Gherardi, G., Nogara, L., Ciciliot, S., Fadini, G. P., Blaauw, B., Braghetta, P., Bonaldo, P., De Stefani, D., Rizzuto, R., and Mammucari, C. (2018) Loss of mitochondrial calcium uniporter rewires skeletal muscle metabolism and substrate preference. *Cell Death Differ.* **26**, 362–381
 35. Chvanov, M., Voronina, S., Zhang, X., Telnova, S., Chard, R., Ouyang, Y., Armstrong, J., Tanton, H., Awais, M., Latawiec, D., Sutton, R., Criddle, D. N., and Tepikin, A. V. (2020) Knockout of the mitochondrial calcium uniporter strongly suppresses stimulus-metabolism coupling in pancreatic acinar cells but does not reduce severity of experimental acute pancreatitis. *Cells* **9**, 1407
 36. Georgiadou, E., Haythorne, E., Dickerson, M. T., Lopez-Noriega, L., Pullen, T. J., da Silva Xavier, G., Davis, S. P. X., Martinez-Sanchez, A., Semplici, F., Rizzuto, R., McGinty, J. A., French, P. M., Cane, M. C., Jacobson, D. A., Leclerc, I., et al. (2020) The pore-forming subunit MCU of the mitochondrial Ca(2+) uniporter is required for normal glucose-stimulated insulin secretion *in vitro* and *in vivo* in mice. *Diabetologia* **63**, 1368–1381
 37. Flicker, D., Sancak, Y., Mick, E., Goldberger, O., and Mootha, V. K. (2019) Exploring the *in vivo* role of the mitochondrial calcium uniporter in brown fat bioenergetics. *Cell Rep.* **27**, 1364–1375.e5
 38. Bisbach, C. M., Hutto, R. A., Poria, D., Clegghorn, W. M., Abbas, F., Vinberg, F., Kefalov, V. J., Hurley, J. B., and Brockerhoff, S. E. (2020) Mitochondrial calcium uniporter (MCU) deficiency reveals an alternate path for Ca(2+) uptake in photoreceptor mitochondria. *Sci. Rep.* **10**, 16041
 39. Altamimi, T. R., Karwi, Q. G., Uddin, G. M., Fukushima, A., Kwong, J. Q., Molkentin, J. D., and Lopaschuk, G. D. (2019) Cardiac-specific deficiency of the mitochondrial calcium uniporter augments fatty acid oxidation and functional reserve. *J. Mol. Cell. Cardiol.* **127**, 223–231
 40. Tomar, D., Jana, F., Dong, Z., Quinn, W. J., 3rd, Jadya, P., Breves, S. L., Daw, C. C., Srikantan, S., Shanmughapriya, S., Nemani, N., Carvalho, E., Tripathi, A., Worth, A. M., Zhang, X., Razmpour, R., et al. (2019) Blockade of MCU-mediated Ca(2+) uptake perturbs lipid metabolism via PP4-dependent AMPK dephosphorylation. *Cell Rep.* **26**, 3709–3725.e7
 41. Gu, L., Larson Casey, J. L., Andrabi, S. A., Lee, J. H., Meza-Perez, S., Randall, T. D., and Carter, A. B. (2019) Mitochondrial calcium uniporter regulates PGC-1alpha expression to mediate metabolic reprogramming in pulmonary fibrosis. *Redox Biol.* **26**, 101307
 42. Hall, D. D., Wu, Y., Domann, F. E., Spitz, D. R., and Anderson, M. E. (2014) Mitochondrial calcium uniporter activity is dispensable for MDA-MB-231 breast carcinoma cell survival. *PLoS One* **9**, e96866
 43. Ren, T., Zhang, H., Wang, J., Zhu, J., Jin, M., Wu, Y., Guo, X., Ji, L., Huang, Q., Yang, H., and Xing, J. (2017) MCU-dependent mitochondrial

- Ca(2+) inhibits NAD(+)/SIRT3/SOD2 pathway to promote ROS production and metastasis of HCC cells. *Oncogene* **36**, 5897–5909
44. Liu, Y., Jin, M., Wang, Y., Zhu, J., Tan, R., Zhao, J., Ji, X., Jin, C., Jia, Y., Ren, T., and Xing, J. (2020) MCU-induced mitochondrial calcium uptake promotes mitochondrial biogenesis and colorectal cancer growth. *Signal Transduct. Target Ther.* **5**, 59
 45. Tarasov, A. I., Semplici, F., Ravier, M. A., Bellomo, E. A., Pullen, T. J., Gilon, P., Sekler, I., Rizzuto, R., and Rutter, G. A. (2012) The mitochondrial Ca²⁺ uniporter MCU is essential for glucose-induced ATP increases in pancreatic beta-cells. *PLoS One* **7**, e39722
 46. Koval, O. M., Nguyen, E. K., Santhana, V., Fidler, T. P., Sebag, S. C., Rasmussen, T. P., Mittauer, D. J., Strack, S., Goswami, P. C., Abel, E. D., and Grumbach, I. M. (2019) Loss of MCU prevents mitochondrial fusion in G1-S phase and blocks cell cycle progression and proliferation. *Sci. Signal.* **12**, eaav1439
 47. Lombardi, A. A., Gibb, A. A., Arif, E., Kolmetzky, D. W., Tomar, D., Luongo, T. S., Jadia, P., Murray, E. K., Lorkiewicz, P. K., Hajnoczky, G., Murphy, E., Arany, Z. P., Kelly, D. P., Margulies, K. B., Hill, B. G., et al. (2019) Mitochondrial calcium exchange links metabolism with the epigenome to control cellular differentiation. *Nat. Commun.* **10**, 4509
 48. Sancak, Y., Markhard, A. L., Kitami, T., Kovacs-Bogdan, E., Kamer, K. J., Udeshi, N. D., Carr, S. A., Chaudhuri, D., Clapham, D. E., Li, A. A., Calvo, S. E., Goldberger, O., and Mootha, V. K. (2013) EMRE is an essential component of the mitochondrial calcium uniporter complex. *Science* **342**, 1379–1382
 49. Zhao, Y., Araki, S., Wu, J., Teramoto, T., Chang, Y. F., Nakano, M., Abdelfattah, A. S., Fujiwara, M., Ishihara, T., Nagai, T., and Campbell, R. E. (2011) An expanded palette of genetically encoded Ca(2+)-indicators. *Science* **333**, 1888–1891
 50. Pan, X., Liu, J., Nguyen, T., Liu, C., Sun, J., Teng, Y., Fergusson, M. M., Rovira, I. I., Allen, M., Springer, D. A., Aponte, A. M., Gucek, M., Balaban, R. S., Murphy, E., and Finkel, T. (2013) The physiological role of mitochondrial calcium revealed by mice lacking the mitochondrial calcium uniporter. *Nat. Cell Biol.* **15**, 1464–1472
 51. Holmstrom, K. M., Pan, X., Liu, J. C., Menazza, S., Liu, J., Nguyen, T. T., Pan, H., Parks, R. J., Anderson, S., Noguchi, A., Springer, D., Murphy, E., and Finkel, T. (2015) Assessment of cardiac function in mice lacking the mitochondrial calcium uniporter. *J. Mol. Cell. Cardiol.* **85**, 178–182
 52. Luongo, T. S., Lambert, J. P., Yuan, A., Zhang, X., Gross, P., Song, J., Shanmughapriya, S., Gao, E., Jain, M., Houser, S. R., Koch, W. J., Cheung, J. Y., Madesh, M., and Elrod, J. W. (2015) The mitochondrial calcium uniporter matches energetic supply with cardiac workload during stress and modulates permeability transition. *Cell Rep.* **12**, 23–34
 53. Kwong, J. Q., Lu, X., Correll, R. N., Schwanekamp, J. A., Vagnozzi, R. J., Sargent, M. A., York, A. J., Zhang, J., Bers, D. M., and Molkenin, J. D. (2015) The mitochondrial calcium uniporter selectively matches metabolic output to acute contractile stress in the heart. *Cell Rep.* **12**, 15–22
 54. Williamson, D. H., Lund, P., and Krebs, H. A. (1967) The redox state of free nicotinamide-adenine dinucleotide in the cytoplasm and mitochondria of rat liver. *Biochem. J.* **103**, 514–527
 55. Nichols, M., Elustondo, P. A., Warford, J., Thirumaran, A., Pavlov, E. V., and Robertson, G. S. (2017) Global ablation of the mitochondrial calcium uniporter increases glycolysis in cortical neurons subjected to energetic stressors. *J. Cereb. Blood Flow Metab.* **37**, 3027–3041
 56. Kwong, J. Q., Huo, J., Bround, M. J., Boyer, J. G., Schwanekamp, J. A., Ghazal, N., Maxwell, J. T., Jang, Y. C., Khuchua, Z., Shi, K., Bers, D. M., Davis, J., and Molkenin, J. D. (2018) The mitochondrial calcium uniporter underlies metabolic fuel preference in skeletal muscle. *JCI Insight* **3**, e121689
 57. Li, Y., and Chen, Y. (2019) AMPK and autophagy. *Adv. Exp. Med. Biol.* **1206**, 85–108
 58. Yoshii, S. R., and Mizushima, N. (2017) Monitoring and measuring autophagy. *Int. J. Mol. Sci.* **18**, 1865
 59. Jang, C., Chen, L., and Rabinowitz, J. D. (2018) Metabolomics and isotope tracing. *Cell* **173**, 822–837
 60. DeBerardinis, R. J., Mancuso, A., Daikhin, E., Nissim, I., Yudkoff, M., Wehrli, S., and Thompson, C. B. (2007) Beyond aerobic glycolysis: Transformed cells can engage in glutamine metabolism that exceeds the requirement for protein and nucleotide synthesis. *Proc. Natl. Acad. Sci. U. S. A.* **104**, 19345–19350
 61. Lemons, J. M., Feng, X. J., Bennett, B. D., Legesse-Miller, A., Johnson, E. L., Raitman, I., Pollina, E. A., Rabitz, H. A., Rabinowitz, J. D., and Collier, H. A. (2010) Quiescent fibroblasts exhibit high metabolic activity. *PLoS Biol.* **8**, e1000514
 62. Metallo, C. M., Gameiro, P. A., Bell, E. L., Mattaini, K. R., Yang, J., Hiller, K., Jewell, C. M., Johnson, Z. R., Irvine, D. J., Guarente, L., Kelleher, J. K., Vander Heiden, M. G., Iliopoulos, O., and Stephanopoulos, G. (2011) Reductive glutamine metabolism by IDH1 mediates lipogenesis under hypoxia. *Nature* **481**, 380–384
 63. Philipp, F. V., Scott, D. A., Ronai, Z. A., Osterman, A. L., and Smith, J. W. (2012) Reverse TCA cycle flux through isocitrate dehydrogenases 1 and 2 is required for lipogenesis in hypoxic melanoma cells. *Pigment Cell Melanoma Res.* **25**, 375–383
 64. Reitzer, L. J., Wice, B. M., and Kennell, D. (1979) Evidence that glutamine, not sugar, is the major energy source for cultured HeLa cells. *J. Biol. Chem.* **254**, 2669–2676
 65. Zheng, J. (2012) Energy metabolism of cancer: Glycolysis versus oxidative phosphorylation. *Oncol. Lett.* **4**, 1151–1157
 66. Henry, O., Jolicoeur, M., and Kamen, A. (2011) Unraveling the metabolism of HEK-293 cells using lactate isotopomer analysis. *Bioproc. Biosyst. Eng.* **34**, 263–273
 67. Dietmair, S., Hodson, M. P., Quek, L. E., Timmins, N. E., Gray, P., and Nielsen, L. K. (2012) A multi-omics analysis of recombinant protein production in Hek293 cells. *PLoS One* **7**, e43394
 68. Aguer, C., Gambarotta, D., Mailloux, R. J., Moffat, C., Dent, R., McPherson, R., and Harper, M. E. (2011) Galactose enhances oxidative metabolism and reveals mitochondrial dysfunction in human primary muscle cells. *PLoS One* **6**, e28536
 69. [preprint] Yoast, R. E., Emrich, S. M., Zhang, X., Xin, P., Arige, V., Pathak, T., Benson, J. C., Johnson, M. T., Lakomski, N., Hempel, N., Han, J. M., Dupont, G., Yule, D. I., Sneyd, J., and Trebak, M. (2021) Regulation of interorganellar Ca²⁺ transfer and NFAT activation by the mitochondrial Ca²⁺ uniporter. *bioRxiv*. <https://doi.org/10.1101/438854>
 70. Midgley, P. J., Rutter, G. A., Thomas, A. P., and Denton, R. M. (1987) Effects of Ca²⁺ and Mg²⁺ on the activity of pyruvate dehydrogenase phosphate phosphatase within toluene-permeabilized mitochondria. *Biochem. J.* **241**, 371–377
 71. McCormack, J. G. (1985) Characterization of the effects of Ca²⁺ on the intramitochondrial Ca²⁺-sensitive enzymes from rat liver and within intact rat liver mitochondria. *Biochem. J.* **231**, 581–595
 72. Sugden, M. C., and Holness, M. J. (2003) Recent advances in mechanisms regulating glucose oxidation at the level of the pyruvate dehydrogenase complex by PDKs. *Am. J. Physiol. Endocrinol. Metab.* **284**, E855–862
 73. Rasmussen, T. P., Wu, Y., Joiner, M. L., Koval, O. M., Wilson, N. R., Luczak, E. D., Wang, Q., Chen, B., Gao, Z., Zhu, Z., Wagner, B. A., Soto, J., McCormick, M. L., Kutschke, W., Weiss, R. M., et al. (2015) Inhibition of MCU forces extramitochondrial adaptations governing physiological and pathological stress responses in heart. *Proc. Natl. Acad. Sci. U. S. A.* **112**, 9129–9134
 74. Tilton, W. M., Seaman, C., Carriero, D., and Piomelli, S. (1991) Regulation of glycolysis in the erythrocyte: Role of the lactate/pyruvate and NAD/NADH ratios. *J. Lab. Clin. Med.* **118**, 146–152
 75. Cerdan, S., Rodrigues, T. B., Sierra, A., Benito, M., Fonseca, L. L., Fonseca, C. P., and Garcia-Martin, M. L. (2006) The redox switch/redox coupling hypothesis. *Neurochem. Int.* **48**, 523–530
 76. Yellen, G. (2018) Fueling thought: Management of glycolysis and oxidative phosphorylation in neuronal metabolism. *J. Cell Biol.* **217**, 2235–2246
 77. Patgiri, A., Skinner, O. S., Miyazaki, Y., Schleifer, G., Marutani, E., Shah, H., Sharma, R., Goodman, R. P., To, T. L., Robert Bao, X., Ichinose, F., Zapol, W. M., and Mootha, V. K. (2020) An engineered enzyme that targets circulating lactate to alleviate intracellular NADH:NAD(+) imbalance. *Nat. Biotechnol.* **38**, 309–313
 78. Jeon, S. M. (2016) Regulation and function of AMPK in physiology and diseases. *Exp. Mol. Med.* **48**, e245

Metabolic adaptation to loss of calcium signaling

79. Zhang, J., Pavlova, N. N., and Thompson, C. B. (2017) Cancer cell metabolism: The essential role of the nonessential amino acid, glutamine. *EMBO J.* **36**, 1302–1315
80. Mullen, A. R., Hu, Z., Shi, X., Jiang, L., Boroughs, L. K., Kovacs, Z., Boriack, R., Rakheja, D., Sullivan, L. B., Linehan, W. M., Chandel, N. S., and DeBerardinis, R. J. (2014) Oxidation of alpha-ketoglutarate is required for reductive carboxylation in cancer cells with mitochondrial defects. *Cell Rep.* **7**, 1679–1690
81. Wise, D. R., Ward, P. S., Shay, J. E., Cross, J. R., Gruber, J. J., Sachdeva, U. M., Platt, J. M., DeMatteo, R. G., Simon, M. C., and Thompson, C. B. (2011) Hypoxia promotes isocitrate dehydrogenase-dependent carboxylation of alpha-ketoglutarate to citrate to support cell growth and viability. *Proc. Natl. Acad. Sci. U. S. A.* **108**, 19611–19616
82. Gaude, E., Schmidt, C., Gammage, P. A., Dugourd, A., Blacker, T., Chew, S. P., Saez-Rodriguez, J., O'Neill, J. S., Szabadkai, G., Minczuk, M., and Frezza, C. (2018) NADH shuttling couples cytosolic reductive carboxylation of glutamine with glycolysis in cells with mitochondrial dysfunction. *Mol. Cell* **69**, 581–593.e7
83. To, T. L., Cuadros, A. M., Shah, H., Hung, W. H. W., Li, Y., Kim, S. H., Rubin, D. H. F., Boe, R. H., Rath, S., Eaton, J. K., Piccioni, F., Goodale, A., Kalani, Z., Doench, J. G., Root, D. E., *et al.* (2019) A compendium of genetic modifiers of mitochondrial dysfunction reveals intra-organellar buffering. *Cell* **179**, 1222–1238
84. Brodsky, A. N., Odenwelder, D. C., and Harcum, S. W. (2019) High extracellular lactate causes reductive carboxylation in breast tissue cell lines grown under normoxic conditions. *PLoS One* **14**, e0213419
85. Filadi, R., Leal, N. S., Schreiner, B., Rossi, A., Dentoni, G., Pinho, C. M., Wiehager, B., Cieri, D., Cali, T., Pizzo, P., and Ankarcrona, M. (2018) TOM70 Sustains cell bioenergetics by promoting IP3R3-mediated ER to mitochondria Ca(2+) transfer. *Curr. Biol.* **28**, 369–382.e6
86. Kania, E., Roest, G., Vervliet, T., Parys, J. B., and Bultynck, G. (2017) IP3 receptor-mediated calcium signaling and its role in autophagy in cancer. *Front. Oncol.* **7**, 140
87. Bootman, M. D., Chehab, T., Bultynck, G., Parys, J. B., and Rietdorf, K. (2018) The regulation of autophagy by calcium signals: Do we have a consensus? *Cell Calcium* **70**, 32–46
88. Arroyo, J. D., Jourdain, A. A., Calvo, S. E., Ballarano, C. A., Doench, J. G., Root, D. E., and Mootha, V. K. (2016) A genome-wide CRISPR death screen identifies genes essential for oxidative phosphorylation. *Cell Metab.* **24**, 875–885
89. Mackrill, J. J. (2012) Ryanodine receptor calcium release channels: An evolutionary perspective. *Adv. Exp. Med. Biol.* **740**, 159–182
90. Garcia, C. R. S., Alves, E., Pereira, P. H. S., Bartlett, P. J., Thomas, A. P., Mikoshiba, K., Plattner, H., and Sibley, L. D. (2017) InsP3 signaling in Apicomplexan parasites. *Curr. Top. Med. Chem.* **17**, 2158–2165
91. Alzayady, K. J., Sebe-Pedros, A., Chandrasekhar, R., Wang, L., Ruiz-Trillo, I., and Yule, D. I. (2015) Tracing the evolutionary history of inositol, 1, 4, 5-trisphosphate receptor: Insights from analyses of *Capaspora owczarzaki* Ca²⁺ release channel orthologs. *Mol. Biol. Evol.* **32**, 2236–2253
92. Bick, A. G., Calvo, S. E., and Mootha, V. K. (2012) Evolutionary diversity of the mitochondrial calcium uniporter. *Science* **336**, 886
93. Arduino, D. M., Wettmarshausen, J., Vais, H., Navas-Navarro, P., Cheng, Y., Leimpek, A., Ma, Z., Delrio-Lorenzo, A., Giordano, A., Garcia-Perez, C., Medard, G., Kuster, B., Garcia-Sancho, J., Mokranjac, D., Foskett, J. K., *et al.* (2017) Systematic identification of MCU Modulators by orthogonal interspecies chemical screening. *Mol. Cell* **67**, 711–723.e7
94. Woods, J. J., and Wilson, J. J. (2020) Inhibitors of the mitochondrial calcium uniporter for the treatment of disease. *Curr. Opin. Chem. Biol.* **55**, 9–18
95. Kon, N., Murakoshi, M., Isobe, A., Kagechika, K., Miyoshi, N., and Nagayama, T. (2017) DS16570511 is a small-molecule inhibitor of the mitochondrial calcium uniporter. *Cell Death Discov.* **3**, 17045
96. Blake, D. A., and McLean, N. V. (1989) A colorimetric assay for the measurement of D-glucose consumption by cultured cells. *Anal. Biochem.* **177**, 156–160
97. Hohorst, H. J. (1965) *Methods in Enzymatic Analysis*, 2nd ed., Academic Press, NY
98. Zhu, A., Romero, R., and Petty, H. R. (2010) A sensitive fluorimetric assay for pyruvate. *Anal. Biochem.* **396**, 146–151
99. Davila, A., Liu, L., Chellappa, K., Redpath, P., Nakamaru-Ogiso, E., Paoletta, L. M., Zhang, Z., Migaud, M. E., Rabinowitz, J. D., and Baur, J. A. (2018) Nicotinamide adenine dinucleotide is transported into mammalian mitochondria. *ELife* **7**, e33246
100. Zhu, A., Romero, R., and Petty, H. R. (2009) An enzymatic fluorimetric assay for glucose-6-phosphate: Application in an *in vitro* Warburg-like effect. *Anal. Biochem.* **388**, 97–101
101. Lust, W. D., Feussner, G. K., Barbehenn, E. K., and Passonneau, J. V. (1981) The enzymatic measurement of adenine nucleotides and P-creatine in picomole amounts. *Anal. Biochem.* **110**, 258–266
102. Casciano, J. C., Perry, C., Cohen-Nowak, A. J., Miller, K. D., Vande Voorde, J., Zhang, Q., Chalmers, S., Sandison, M. E., Liu, Q., Hedley, A., McBryan, T., Tang, H. Y., Gorman, N., Beer, T., Speicher, D. W., *et al.* (2020) MYC regulates fatty acid metabolism through a multigenic program in claudin-low triple negative breast cancer. *Br. J. Cancer* **122**, 868–884
103. Kim, S., Kim, D., Cho, S. W., Kim, J., and Kim, J. S. (2014) Highly efficient RNA-guided genome editing in human cells *via* delivery of purified Cas9 ribonucleoproteins. *Genome Res.* **24**, 1012–1019
104. Jacobi, A. M., Rettig, G. R., Turk, R., Collingwood, M. A., Zeiner, S. A., Quadros, R. M., Harms, D. W., Bonthuis, P. J., Gregg, C., Ohtsuka, M., Gurumurthy, C. B., and Behlke, M. A. (2017) Simplified CRISPR tools for efficient genome editing and streamlined protocols for their delivery into mammalian cells and mouse zygotes. *Methods* **121-122**, 16–28